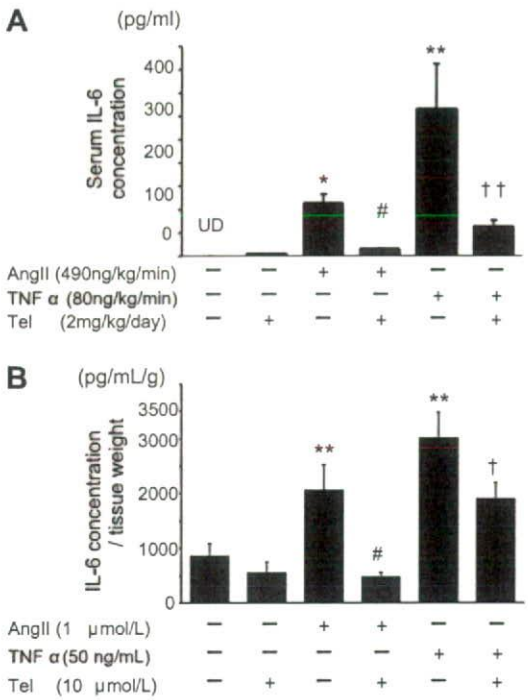

Figure 6. Telmisartan attenuated IL-6 production in vivo and ex vivo. A, Serum concentration of IL-6 was measured in mice injected with Ang II (490 ng/kg per minute) or TNF-α (80 ng/kg per minute) in the presence or absence of telmisartan (Tel; 2 mg/kg per day) administration for 1 week (No. of independent experiments was 5). *P<0.05; **P<0.01 vs control (no treatment); #P<0.05 vs Ang II; ††P<0.01 vs TNF-α. UD indicates undetectable. B, An aortic segment was stimulated ex vivo with Ang II (1 μmol/L) or TNF-α (50 ng/mL) in the presence or absence of Tel (10 μmol/L) in DMEM supplemented with 0.1% BSA for 48 hours. The concentration of IL-6 in the supernatant was measured and normalized with wet weight of the aortic segment (No. of independent experiment was 4 in duplicate). **P<0.01 vs control; #P<0.05 vs Ang II; †P<0.05 vs TNF-α.

tion of TNF-α–induced NF-κB DNA binding. In contrast, activated PPARγ physically interacted with C/EBPβ, suggesting that this protein–protein interaction attenuates the DNA binding of C/EBPβ. Although the precise mechanisms are not clear at this point, it may be possible that telmisartan inhibits NF-κB and C/EBPβ DNA binding activity through the same mechanism.

Inflammation plays a crucial role in the initiation and progression of atherosclerosis.[26] IL-6 enhanced VSMC growth induced by platelet-derived growth factor.[27] IL-6 also increased both monocyte chemoattractant protein-1 production and DNA synthesis of VSMCs, which may coordinate inflammatory and proliferative responses.[28] IL-6 is also a useful biomarker predicting future cardiovascular events.[29] TNF-α also enhances vascular inflammation. Blockade of TNF-α activity by soluble TNF-α receptor suppressed coronary artery neointimal formation after cardiac transplantation in rabbits.[30] Therefore, telmisartan inhibition of TNF-α–induced IL-6 expression, which was not observed by valsartan, may attenuate vascular inflammation.

A recent report showed that C/EBPβ was involved in IL-17–induced C-reactive protein expression in VSMCs.[31] Another report showed that C/EBPβ regulated monocyte chemoattractant protein-1 expression in the aorta of hyperinsulinemic rats.[32] These studies suggest that C/EBPβ is also involved in vascular inflammation. Because NF-κB is well known to regulate gene expression of various inflammatory molecules,[33] telmisartan inhibition of NF-κB and C/EBPβ may contribute to attenuation of a broad range of inflammatory responses of blood vessel. However, it is not clear at this point whether telmisartan modulates gene expression induced by TNF-α other than IL-6 induction.

TZDs were constantly reported to inhibit atherogenesis in various models. Rosiglitazone inhibited development of atherosclerosis in LDL receptor–deficient mice.[11] Rosiglitazone was also shown to have additive effects on plaque regression in the combination treatment with simvastatin in an atherosclerotic rabbit model.[34] AT1R antagonists were also reported to suppress atherogenesis. Strawn et al demonstrated that losartan attenuated atherogenesis in monkeys with hypercholesterolemia.[35] Based on these studies and our results, telmisartan may be more protective against vascular lesion formation attributable to PPARγ activation and AT1R antagonism.

Perspective

In the present study, we showed that telmisartan inhibited Ang II– as well as TNF-α–induced IL-6 expression in VSMCs, rat aorta, and mice. Inhibition of TNF-α–induced IL-6 expression was mediated by PPARγ. And inhibition of NF-κB and C/EBPβ DNA binding by telmisartan may be responsible for suppression of TNF-α–induced IL-6 expression. The dual inhibition (Ang II– and TNF-α–induced IL-6 expression) of the inflammatory cytokine production by telmisartan may be beneficial for treatment of not only hypertension but also atherosclerotic cardiovascular diseases. However, large clinical trials are needed to determine whether these unique properties of telmisartan cause better clinical outcome in cardiovascular disease prevention.

Sources of Funding

This study was supported in part by grants-in-aid for scientific research from the Ministry of Education, Culture, Sports, Science and Technology of Japan (19590867; T.I.). Q.T. was supported by the Japan–China Sasakawa Medical Fellowship.

Disclosures

None.

References

1. de Gasparo M, Catt KJ, Inagami T, Wright JW, Unger T. International union of pharmacology. XXIII. The angiotensin II receptors. *Pharmacol Rev.* 2000;52:415–472.
2. Ferrario CM. Role of angiotensin II in cardiovascular disease therapeutic implications of more than a century of research. *J Renin Angiotensin Aldosterone Syst.* 2006;7:3–14.
3. McMurray JJ, Ostergren J, Swedberg K, Granger CB, Held P, Michelson EL, Olofsson B, Yusuf S, Pfeffer MA. Effects of candesartan in patients with chronic heart failure and reduced left-ventricular systolic function taking angiotensin-converting-enzyme inhibitors: the CHARM-Added trial. *Lancet.* 2003;362:767–771.
4. Barnett AH, Bain SC, Bouter P, Karlberg B, Madsbad S, Jervell J, Mustonen J. Angiotensin-receptor blockade versus converting-enzyme inhibition in type 2 diabetes and nephropathy. *N Engl J Med.* 2004;351:1952–1961.

5. Pfeffer MA, McMurray JJ, Velazquez EJ, Rouleau JL, Kober L, Maggioni AP, Solomon SD, Swedberg K, Van de Werf F, White H, Leimberger JD, Henis M, Edwards S, Zelenkofske S, Sellers MA, Califf RM. Valsartan, captopril, or both in myocardial infarction complicated by heart failure, left ventricular dysfunction, or both. *N Engl J Med.* 2003; 349:1893–1906.
6. Gillespie EL, White CM, Kardas M, Lindberg M, Coleman CI. The impact of ACE inhibitors or angiotensin II type 1 receptor blockers on the development of new-onset type 2 diabetes. *Diabetes Care.* 2005;28: 2261–2266.
7. Healey JS, Baranchuk A, Crystal E, Morillo CA, Garfinkle M, Yusuf S, Connolly SJ. Prevention of atrial fibrillation with angiotensin-converting enzyme inhibitors and angiotensin receptor blockers: a meta-analysis. *J Am Coll Cardiol.* 2005;45:1832–1839.
8. Schupp M, Janke J, Clasen R, Unger T, Kintscher U. Angiotensin type 1 receptor blockers induce peroxisome proliferator-activated receptor-gamma activity. *Circulation.* 2004;109:2054–2057.
9. Benson SC, Pershadsingh HA, Ho CI, Chittiboyina A, Desai P, Pravenec M, Qi N, Wang J, Avery MA, Kurtz TW. Identification of telmisartan as a unique angiotensin II receptor antagonist with selective PPARgamma-modulating activity. *Hypertension.* 2004;43:993–1002.
10. Yki-Jarvinen H.Thiazolidinediones. *N Engl J Med.* 2004;351:1106–1118.
11. Li AC, Brown KK, Silvestre MJ, Willson TM, Palinski W, Glass CK. Peroxisome proliferator-activated receptor gamma ligands inhibit development of atherosclerosis in LDL receptor-deficient mice. *J Clin Invest.* 2000;106:523–531.
12. Pascual G, Fong AL, Ogawa S, Gamliel A, Li AC, Perissi V, Rose DW, Willson TM, Rosenfeld MG, Glass CK. A SUMOylation-dependent pathway mediates transrepression of inflammatory response genes by PPAR-gamma. *Nature.* 2005;437:759–763.
13. Wang Z, Castresana MR, Newman WH. NF-kappaB is required for TNF-alpha-directed smooth muscle cell migration. *FEBS Lett.* 2001;508: 360–364.
14. Funakoshi Y, Ichiki T, Ito K, Takeshita A. Induction of interleukin-6 expression by angiotensin II in rat vascular smooth muscle cells. *Hypertension.* 1999;34:118–125.
15. Lobbes MB, Lutgens E, Heeneman S, Cleutjens KB, Kooi ME, van Engelshoven JM, Daemen MJ, Nelemans PJ. Is there more than C-reactive protein and fibrinogen? The prognostic value of soluble CD40 ligand, interleukin-6 and oxidized low-density lipoprotein with respect to coronary and cerebral vascular disease. *Atherosclerosis.* 2006;187:18–25.
16. Fujita K, Yoneda M, Wada K, Mawatari H, Takahashi H, Kirikoshi H, Inamori M, Nozaki Y, Maeyama S, Saito S, Iwasaki T, Terauchi Y, Nakajima A. Telmisartan, an angiotensin II type 1 receptor blocker, controls progress of nonalcoholic steatohepatitis in rats. *Dig Dis Sci.* 2007;52:3455–3464.
17. Link A, Lenz M, Legner D, Böhm M, Nickenig G. Telmisartan inhibits beta2-integrin MAC-1 expression in human T-lymphocytes. *J Hypertens.* 2006;24:1891–1898.
18. Northemann W, Braciak TA, Hattori M, Lee F, Fey GH. Structure of the rat interleukin 6 gene and its expression in macrophage-derived cells. *J Biol Chem.* 1989;264:16072–16082.
19. Stangier J, Su CA, Roth W. Pharmacokinetics of orally and intravenously administered telmisartan in healthy young and elderly volunteers and in hypertensive patients. *J Int Med Res.* 2000;28:149–167.
20. Dendorfer U, Oettgen P, Libermann TA. Multiple regulatory elements in the interleukin-6 gene mediate induction by prostaglandins, cyclic AMP, and lipopolysaccharide. *Mol Cell Biol.* 1994;14:4443–4454.
21. Brown JD, Plutzky J. Peroxisome proliferator-activated receptors as transcriptional nodal points and therapeutic targets. *Circulation.* 2007;115: 518–533.
22. Glass CK, Ogawa S. Combinatorial roles of nuclear receptors in inflammation and immunity. *Nat Rev Immunol.* 2006;6:44–55.
23. Ruan H, Pownall HJ, Lodish HF. Troglitazone antagonizes tumor necrosis factor-alpha-induced reprogramming of adipocyte gene expression by inhibiting the transcriptional regulatory functions of NF-kappaB. *J Biol Chem.* 2003;278:28181–28192.
24. Takata Y, Kitami Y, Yang ZH, Nakamura M, Okura T, Hiwada K. Vascular inflammation is negatively autoregulated by interaction between CCAAT/enhancer-binding protein-delta and peroxisome proliferator-activated receptor-gamma. *Circ Res.* 2002;91:427–433.
25. Wang LH, Yang XY, Zhang X, Farrar WL. Inhibition of adhesive interaction between multiple myeloma and bone marrow stromal cells by PPARgamma crosstalk with NF-kappaB and c/EBPbeta. *Blood.* 2007; 110:4373–4384.
26. Ross R. Atherosclerosis–an inflammatory disease. *N Engl J Med.* 1999; 340:115–126.
27. Ikeda U, Ikeda M, Oohara T, Oguchi A, Kamitani T, Tsuruya Y, Kano S. Interleukin 6 stimulates growth of vascular smooth muscle cells in a PDGF-dependent manner. *Am J Physiol.* 1991;260:H1713–H1717.
28. Watanabe S, Mu W, Kahn A, Jing N, Li JH, Lan HY, Nakagawa T, Ohashi R, Johnson RJ. Role of JAK/STAT pathway in IL-6-induced activation of vascular smooth muscle cells. *Am J Nephrol.* 2004;24: 387–392.
29. Koenig W, Khuseyinova N. Biomarkers of atherosclerotic plaque instability and rupture. *Arterioscler Thromb Vasc Biol.* 2007;27:15–26.
30. Clausell N, Molossi S, Sett S, Rabinovitch M. In vivo blockade of tumor necrosis factor-alpha in cholesterol-fed rabbits after cardiac transplant inhibits acute coronary artery neointimal formation. *Circulation.* 1994; 89:2768–2779.
31. Patel DN, King CA, Bailey SR, Holt JW, Venkatachalam K, Agrawal A, Valente AJ, Chandrasekar B. Interleukin-17 stimulates C-reactive protein expression in hepatocytes and smooth muscle cells via p38 MAPK and ERK1/2-dependent NF-kappaB and C/EBPbeta activation. *J Biol Chem.* 2007;282:27229–27238.
32. Sato Y, Nishio Y, Sekine O, Kodama K, Nagai Y, Nakamura T, Maegawa H, Kashiwagi A. Increased expression of CCAAT/enhancer binding protein-beta and -delta and monocyte chemoattractant protein-1 genes in aortas from hyperinsulinaemic rats. *Diabetologia.* 2007;50:481–489.
33. de Winther MP, Kanters E, Kraal G, Hofker MH. Nuclear factor kappaB signaling in atherogenesis. *Arterioscler Thromb Vasc Biol.* 2005;25: 904–914.
34. Phillips JW, Barringhaus KG, Sanders JM, Yang Z, Chen M, Hesselbacher S, Czarnik AC, Ley K, Nadler J, Sarembock IJ. Rosiglitazone reduces the accelerated neointima formation after arterial injury in a mouse injury model of type 2 diabetes. *Circulation.* 2003;108: 1994–1999.
35. Strawn WB, Chappell MC, Dean RH, Kivlighn S, Ferrario CM. Inhibition of early atherogenesis by losartan in monkeys with diet-induced hypercholesterolemia. *Circulation.* 2000;101:1586–1593.

INTERNAL MEDICINE

□ CASE REPORT □

Chest Pain without Significant Coronary Stenosis after Implantation of Sirolimus-Eluting Stents

Ken-ichi Hiasa[1], Masao Takemoto[1], Ryuichi Matsukawa[1], Tetsuya Matoba[1], Takeshi Kuga[2] and Kenji Sunagawa[1]

Abstract

We encountered a case of exercise-induced chest pain after the implantation of sirolimus-eluting stents (SESs). She had no history of previous chest pain, and an exercise stress test just after the implantation of the SESs was negative without any symptoms. However, six months after the implantation of the SESs, she began to experience frequent episodes of severe chest pain on effort in spite of there being no significant coronary stenosis. Interestingly, severe coronary vasoconstriction was induced by an intracoronary administration of acetylcholine, and exercise stress testing revealed positive findings with chest pain and ST-T segment depression on ECG. An intensive treatment with two types of calcium channel blockers could readily and completely abolish the exercise-induced chest pain and ST-T segment depression on the ECG. In view of these findings, we presumed that coronary microvessel dysfunction and/or exercise-induced coronary vasoconstriction leading to myocardial ischemia had appeared 6 months after the implantation of the SESs. Although the pathogenesis of this phenomenon could not be completely elucidated, the anatomical and functional abnormalities of the coronary arteries associated with the implantation of the SESs may have been one of the most important mechanisms.

Key words: coronary intervention, exercise, coronary vasoconstriction, microvessel dysfunction

(Inter Med 48: 213-217, 2009)
(DOI: 10.2169/internalmedicine.48.1581)

Introduction

Sirolimus-eluting stents (SESs) have gained widespread use due to the extraordinarily low rates of restensosis (1). Despite these generally superior clinical outcomes, some adverse effects (2) associated with SES implantations including coronary vasoconstriction (3, 4) and endothelial dysfunction (5) have been reported. We describe a case of exercise-induced chest pain without any significant coronary stenosis 6 months after the implantation of SESs.

Case Report

A 59-year-old woman was admitted to our hospital with increasing episodes of chest pain on effort. She had no history of prior chest symptoms. Her coronary risk factors included a family history of ischemic heart disease, arterial hypertension, and dyslipidemia. Both the electrocardiogram (ECG) and echocardiogram on admission were normal (Fig. 1A). Since the coronary angiogram (CAG) revealed 1 vessel disease with a long, diffuse narrow, and severe stenosis of the proximal and mid left anterior descending (LAD) coronary artery (Fig. 2A), two SESs (Cypher® 3.5×23, 3.0×28 mm, Cordis Corporation, Miami Lakes, FL) were implanted just proximal to the mid LAD lesions (Fig. 2B). After that procedure, she was free of any symptoms and had no significant ECG changes observed during exercise stress testing (Fig. 1B), while being treated with medications including aspirin, ticlopidine, statin, and the calcium channel blocker (CCB), 5 mg per day of amlodipine. Six months after the implantation of the SESs, she began to have frequent episodes of severe chest pain on effort, and then, she was emergently readmitted to our hospital. However, the CAG revealed no restenosis at the SES implantation sites and no significant stenosis of any of the coronary arteries (Fig. 2C).

[1]Department of Cardiovascular Medicine, Kyushu University Hospital, Fukuoka and [2]Internal Medicine, Mitsutake Hospital, Nagasaki
Received for publication August 11, 2008; Accepted for publication October 8, 2008
Correspondence to Dr. Masao Takemoto, matakemo@cardiol.med.kyushu-u.ac.jp

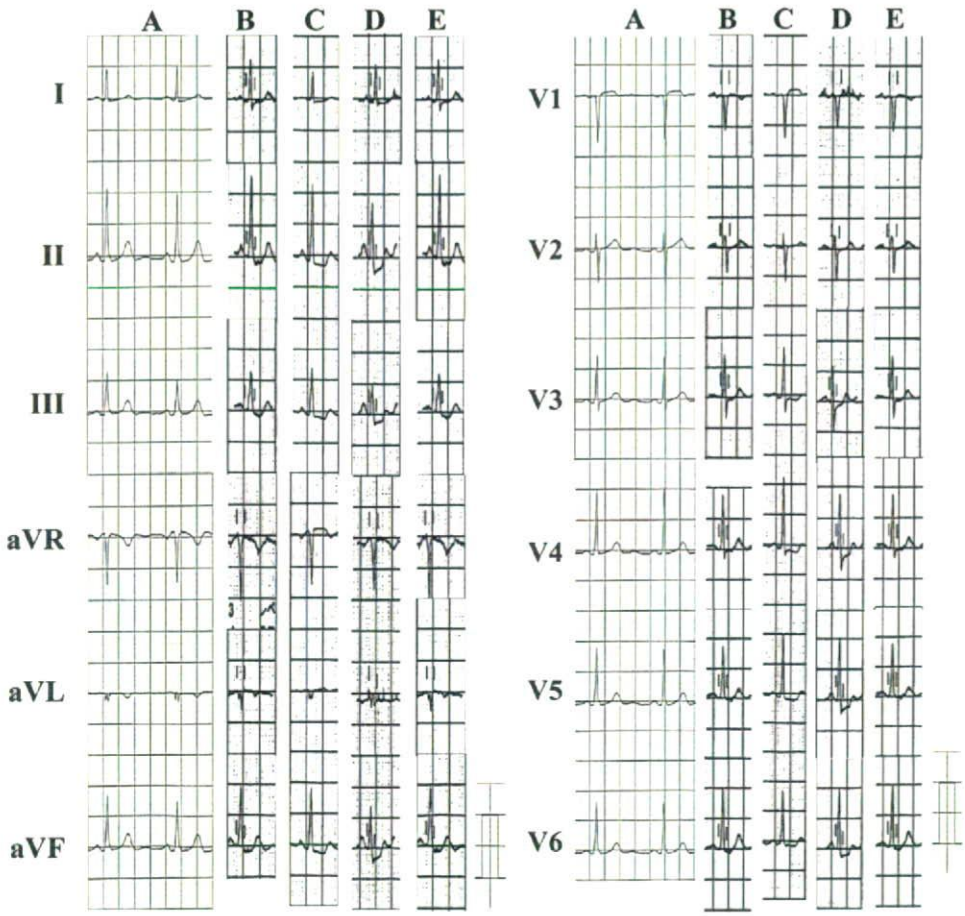

Figure 1. The electrocardiogram on admission (A), during acetylcholine provocation test (C), and during exercise stress testing (B, D, E) just after the implantation of sirolimus-eluting stents (B), under the oral administration of 5 mg per day of benidipine (D), and under intensive treatment with the oral administration of 5 mg per day of benidipine and 100 mg per day of diltiazem (E). The rate-pressure products exceeded 20,000 mmHg×beats/min during each exercise stress testing (B, D, E).

In order to evaluate her coronary vasoconstriction, an intracoronary administration of 30 μg of acetylcholine was performed, yielding severe coronary vasoconstrictions (Fig. 2D) at the distal portion of the site of the implantation of the SES, associated with significant ST depression in the surface ECG leads II, III, aVF, and V3-6 (Fig. 1C) and severe chest pain, even though she had been receiving an oral administration of 5 mg per day of amlodipine. No vasoconstrictive responses were observed in any other coronary artery but LAD. A repeated intracoronary administration of isosorbide dinitrate was able to relieve the coronary vasoconstrictions in accordance with the disappearance of the ST depression in the ECG and chest pain symptoms. With a diagnosis of vasospastic angina, the oral administration of 8 mg per day of benidipine, which has a stronger effect for preventing coronary vasoconstrictions than amlodipine (6) was started in place of amlodipine. However, since she continued to have chest pain associated with significant ST segment depression on the ECG during exercise stress testing (Fig. 1D), intensive CCB treatment with the oral administration of 8 mg per day of benidipine and 100 mg per day of diltiazem was started. The exercise stress test after the intensive CCB treatment, revealed no significant ECG changes or symptoms (Fig. 1E). Since both the exercise stress test and acetylcholine provocation test were positive without significant stenosis in coronary arteries, we presumed that coronary microvessel dysfunction (7, 8) and/or exercise-induced coronary vasoconstrictions leading to myocardial ischemia appeared 6 months after the implantation of the SESs (4). She was completely free of any symptoms thereafter, and has remained well without any symptoms under intensive CCBs treatment for more than 2 years after the implantation of the SESs.

Discussion

We encountered a case of exercise-induced chest pain without significant coronary stenosis 6 months after the implantation of the SESs. The syndrome of chest pain without significant coronary stenosis, but with coronary vasocon-

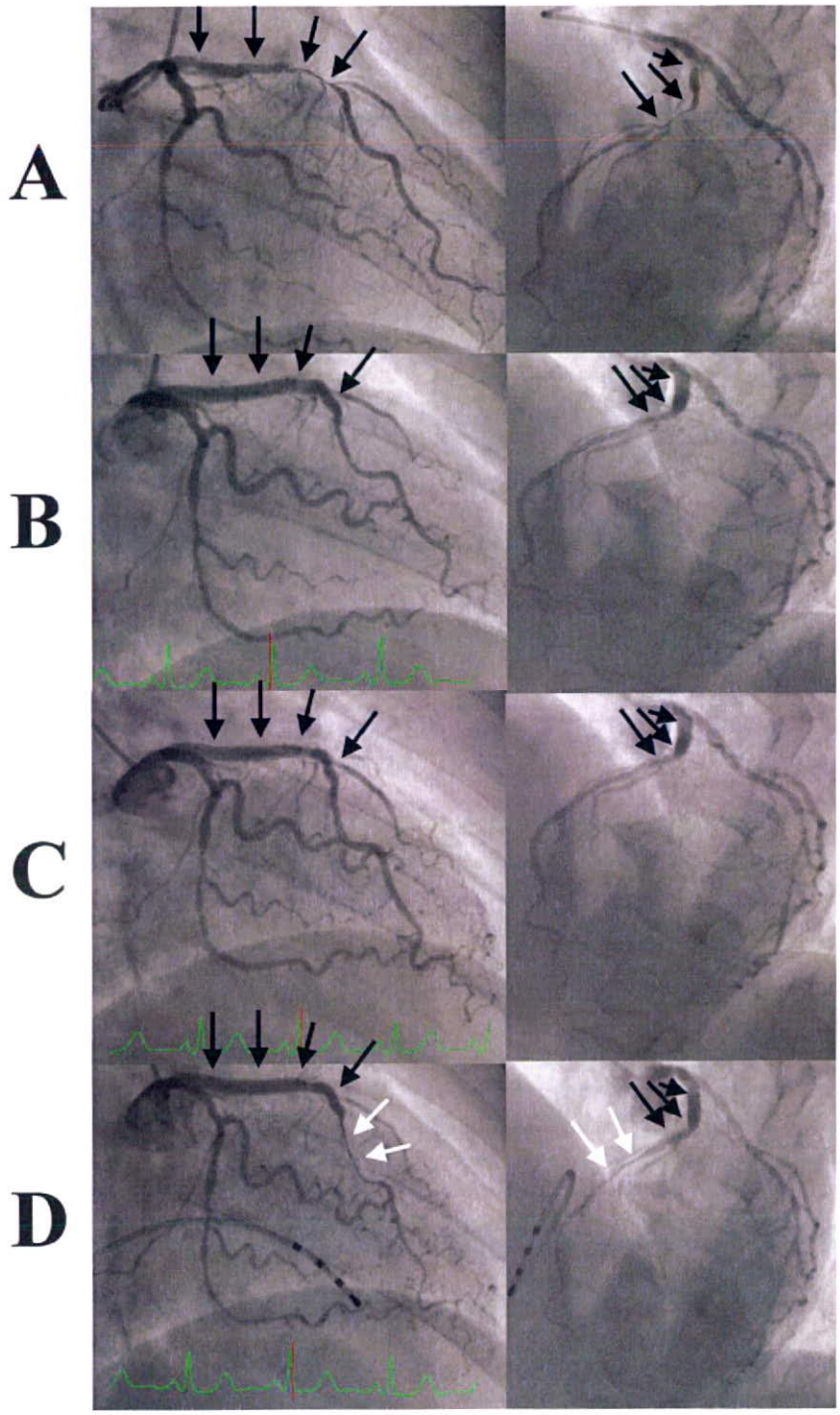

Figure 2. The left coronary angiography in the right (RAO; left panels) and left (LAO; right panels) anterior oblique views obtained before a percutaneous coronary intervention (PCI)(A), just after PCI (B), 6 months after PCI (C), and during an intracoronary administration of acetylcholine (D). The black and white arrows indicate the stent implantation sites and coronary vasoconstriction sites, respectively.

strictions which are induced by acetylcholine or ergonovine maleate, is diagnosed as vasospastic angina. On the other hand, the syndrome of chest pain with a normal CAG is referred to as microvessel dysfunction, the so called cardiac syndrome X (7). The former condition appears to remain common in Japan, and sometimes causes myocardial infarction and cardiac sudden death (9). Both conditions must be rare complications associated with SES implantations, because few case reports have covered that before (4).

Although the pathogenesis of the coronary microvessel dysfunction and vasospastic angina cannot be completely elucidated, endothelial and/or vascular smooth muscle cell

dysfunction has been suggested (10-12). It has been reported that the implantation of the SESs caused both anatomical (13, 14) and functional (5, 15) abnormalities of the coronary arteries. In the angioscopic findings at 6 months after the SES implantations, an incomplete re-endothelialization was observed (14), indicating the existence of impaired endothelial function. Furthermore, the pathologic examination after the implantation of the SES revealed drug or polymer-induced localized vascular inflammatory reactions and/or impaired vessel healing (13, 16, 17). Moreover, an in vitro study showed that sirolimus impairs the endothelium-derived nitric oxide production leading to endothelial dysfunction and hinders the cell viability (5, 15). Finally, enhanced sympathetic nerve stimulation during exercise may accelerate the vasoconstrictor response (smooth muscle cells dysfunction) under the condition of reduced nitric oxide bioavailability (endothelial dysfunction) leading to myocardial ischemia and chest pain. These findings may be one of the important potential mechanisms of exercise-induced coronary microvessel dysfunction and/or vasoconstrictions especially in the late phase after implantation of the SES.

In the present case, the exercise-stress test was negative in the early phase, but became positive, even without significant coronary stenosis, 6 months after the implantation of the SESs. Furthermore, an intracoronary administration of acetylcholine induced coronary vasoconstrictions leading to myocardial ischemia 6 months after the implantation of the SESs. Interestingly, recent clinical trials demonstrated that exercise-induced coronary vasoconstrictions occurred at the adjacent vessel segments of the SES implantation site 6 months after an SES implantation (3), but not in the early phase after SES implantations (18). Although it might have been difficult to observe vasoconstriction at the proximal site of the SES, because the stent was positioned just proximal to LAD, these findings seem to be similar to the clinical course of the present case, and may support the hypothesis that the exercise-induced vasoconstrictions leading to myocardial ischemia had begun to occur 6 months after the SES implantation, in the present case. These conditions may be somewhat drug-refractory, since two types of CCBs were needed to treat it. Moreover, these phenomena were not observed after a biolimus A9-eluting stent (BES) implantation (19). Thus, they may be a specific phenomenon of the SESs. The more complete stent re-endothelialization with BES rather than with SES (19) may be one of the important factors in these phenomena.

Recent clinical trials also have demonstrated that SESs have been associated with an increased rate of myocardial infarctions and death, as compared to the bare metal stents, and this tendency tended to appear 6 months after the SES implantation (20, 21). These results suggest that the coronary vasoconstrictions observed after SES implantations may be one of the important factors in the increased rate of myocardial infarctions and death after the SES implantation, because it has been reported that coronary vasoconstrictions, the so-called "vasospastic angina" sometimes causes myocardial infarctions and cardiac sudden death (9).

To the best of our knowledge, there have been no reports on the exercise-induced chest pain associated with significant ST segment depression on ECG resulting from myocardial ischemia, without significant coronary stenosis after an SES implantation as in this present case. Although the frequency of these abnormalities may be low, physicians should be aware of this condition when examining patients, especially after SES implantation. An intensive CCB treatment may be one of the useful therapeutic strategies for these conditions. Supporting data from clinical and basic trials, however, are required before such conclusions can be made.

Acknowledgement

We thank John Martin for his linguistic assistance with this paper.

References

1. Morice MC, Serruys PW, Sousa JE, et al. A randomized comparison of a sirolimus-eluting stent with a standard stent for coronary revascularization. N Engl J Med **346** (23): 1773-1780, 2002.
2. Daemen J, Wenaweser P, Tsuchida K, et al. Early and late coronary stent thrombosis of sirolimus-eluting and paclitaxel-eluting stents in routine clinical practice: data from a large two-institutional cohort study. Lancet **369** (9562): 667-678, 2007.
3. Togni M, Windecker S, Cocchia R, et al. Sirolimus-eluting stents associated with paradoxic coronary vasoconstriction. J Am Coll Cardiol **46** (2): 231-236, 2005.
4. Maekawa K, Kawamoto K, Fuke S, et al. Images in cardiovascular medicine. Severe endothelial dysfunction after sirolimus-eluting stent implantation. Circulation **113** (23): e850-e851, 2006.
5. Muhlestein JB. Endothelial dysfunction associated with drug-eluting stents what, where, when, and how? J Am Coll Cardiol **51** (22): 2139-2140, 2008.
6. Ito A, Fukumoto Y, Shimokawa H. Changing characteristics of patients with vasospastic angina in the era of new calcium channel blockers. J Cardiovasc Pharmacol **44** (4): 480-485, 2004.
7. Panting JR, Gatehouse PD, Yang GZ, et al. Abnormal subendocardial perfusion in cardiac syndrome X detected by cardiovascular magnetic resonance imaging. N Engl J Med **346** (25): 1948-1953, 2002.
8. Mohri M, Koyanagi M, Egashira K, et al. Angina pectoris caused by coronary microvascular spasm. Lancet **351** (9110): 1165-1169, 1998.
9. Mayer S, Hillis LD. Prinzmetal's variant angina. Clin Cardiol **21** (4): 243-246, 1998.
10. Hurst T, Olson TH, Olson LE, Appleton CP. Cardiac syndrome X and endothelial dysfunction: new concepts in prognosis and treatment. Am J Med **119** (7): 560-566, 2006.
11. Okumura K, Osanai T, Kosugi T, et al. Enhanced phospholipase C activity in the cultured skin fibroblast obtained from patients with coronary spastic angina: possible role for enhanced vasoconstrictor response. J Am Coll Cardiol **36** (6): 1847-1852, 2000.
12. Cox ID, Kaski JC, Clague JR. Endothelial dysfunction in the absence of coronary atheroma causing Prinzmetal's angina. Heart **77** (6): 584, 1997.

13. Joner M, Finn AV, Farb A, et al. Pathology of drug-eluting stents in humans: delayed healing and late thrombotic risk. J Am Coll Cardiol **48** (1): 193-202, 2006.

14. Kotani J, Awata M, Nanto S, et al. Incomplete neointimal coverage of sirolimus-eluting stents: angioscopic findings. J Am Coll Cardiol **47** (10): 2108-2111, 2006.

15. Barilli A, Visigalli R, Sala R, et al. In human endothelial cells rapamycin causes mTORC2 inhibition and impairs cell viability and function. Cardiovasc Res **78** (3): 563-571, 2008.

16. Virmani R, Guagliumi G, Farb A, et al. Localized hypersensitivity and late coronary thrombosis secondary to a sirolimus-eluting stent: should we be cautious? Circulation **109** (6): 701-705, 2004.

17. Nebeker JR, Virmani R, Bennett CL, et al. Hypersensitivity cases associated with drug-eluting coronary stents: a review of available cases from the Research on Adverse Drug Events and Reports (RADAR) project. J Am Coll Cardiol **47** (1): 175-181, 2006.

18. Nakazawa G, Cheng Q, Xu X, Finn AV, Kolodgie FD, Virmani R. Drug-eluting stent implantation may not affect vasomotor function in early phase. J Am Coll Cardiol **51** (11): 1124-1125, 2008.

19. Hamilos MI, Ostojic M, Beleslin B, et al. Differential effects of drug-eluting stents on local endothelium-dependent coronary vasomotion. J Am Coll Cardiol **51** (22): 2123-2129, 2008.

20. Lagerqvist B, James SK, Stenestrand U, Lindback J, Nilsson T, Wallentin L. Long-term outcomes with drug-eluting stents versus bare-metal stents in Sweden. N Engl J Med **356** (10): 1009-1019, 2007.

21. Kastrati A, Mehilli J, Pache J, et al. Analysis of 14 trials comparing sirolimus-eluting stents with bare-metal stents. N Engl J Med **356** (10): 1030-1039, 2007.

Soluble Flt-1 Gene Transfer Ameliorates Neointima Formation After Wire Injury in flt-1 Tyrosine Kinase–Deficient Mice

Jun-ichiro Koga, Tetsuya Matoba, Kensuke Egashira, Mitsuki Kubo, Miho Miyagawa, Eiko Iwata, Katsuo Sueishi, Masabumi Shibuya, Kenji Sunagawa

Objective—We have demonstrated that vascular endothelial growth factor (VEGF) expression is upregulated in injured vascular wall, and blockade of VEGF inhibited monocyte infiltration and neointima formation in several animal models. In the present study, we aimed to clarify relative role of two VEGF receptors, flt-1 versus flk-1/KDR, in neointima formation after injury using flt-1 tyrosine kinase-deficient (Flt-1 $TK^{-/-}$) mice and soluble Flt-1(sFlt-1) gene transfer.

Methods and Results—Neointima formation was comparable between wild-type and Flt-1 $TK^{-/-}$ mice 28 days after intraluminal wire injury in femoral arteries. By contrast, neointima formation was significantly suppressed by sFlt-1 gene transfer into Flt-1 $TK^{-/-}$ mice that blocks VEGF action on flk-1 (intima/media ratio: 2.8 ± 0.4 versus 1.4 ± 0.4, $P<0.05$). The inhibition of neointima formation was preceded by significant reduction of monocyte chemoattractant protein (MCP-1) expression in vascular smooth muscle cells (VSMCs) and monocyte infiltration 7 days after injury. Gene transfer of sFlt-1 or treatment of flk-1–specific antibody significantly inhibited VEGF-induced MCP-1 expression determined by RT-PCR in cultured aortic tissue and VSMCs. MCP-1–induced chemotaxis was equivalent between wild-type and Flt-1 $TK^{-/-}$ mice.

Conclusions—These results suggest that endogenous VEGF accelerates neointima formation through flk-1 by regulating MCP-1 expression in VSMCs and macrophage-mediated inflammation in injured vascular wall in murine model of wire injury. (***Arterioscler Thromb Vasc Biol.* 2009;29:458-464.**)

Key Words: restenosis ■ inflammation ■ smooth muscle cells ■ angiogenesis

Vascular endothelial growth factor (VEGF) is one of the most potent angiogenic and vascular permeability factors playing essential roles in neonatal and postnatal vascular formation. VEGF has gathered growing attention because of its possible contribution to cardiovascular pathophysiology including therapeutic angiogenesis, endothelial regeneration, and inflammation in the vascular wall. VEGF expression is upregulated in human coronary arterial wall after stent implantation, suggesting its role in reendothelialization, perivascular angiogenesis, and neointima formation leading to clinical restenosis.[1] VEGF induction is reproduced in various animal vascular injury models including wire or cuff injury in mice, and balloon injury in rats and rabbits, porcine coronary stent model.[2–4] From these prior studies that supplement or inhibit VEGF pathway in animal models, two conflicting mechanisms have been demonstrated in which VEGF may contribute to neointima formation. One is that VEGF inhibits neointima formation by promoting reendothelialization and inhibiting vascular smooth muscle cell (VSMC) proliferation.[5] The other is that VEGF accelerates neointima formation by promoting inflammation[2,4] and adventitial angiogenesis in the vascular wall.[2,3,6]

In this controversy, clinical studies have been carried out to examine the effect of VEGF gene delivery after percutaneous coronary angioplasty without significant reduction in restenosis.[7–9] Thus, it is crucial to understand the mechanisms underlying differential effects of VEGF during neointima formation to optimize vasculoprotective effects and minimize adverse effects of endogenous VEGF that may depend on receptor, cell type, and the mode of vascular injury including species studied. We have demonstrated that flt-1 (VEGF receptor 1) is upregulated during neointima formation after vascular injury, especially in the neointima, media, and adventitia, and flk-1/KDR (VEGF receptor 2) in the neointima and media, and that blockade of VEGF by soluble Flt-1 (sFlt-1) gene transfer inhibited monocyte infiltration and neointima formation in several animal models.[2,4] However, contribution of each VEGF receptor was not fully clarified in

Received December 2, 2007; revision accepted January 7, 2009.

From the Department of Cardiovascular Medicine (J.K., T.M., K.E., M.K., M.M., E.I., K. Sunagawa) and the Division of Pathophysiological and Experimental Pathology (K. Sueishi), Graduate School of Medical Sciences, Kyushu University, Fukuoka, Japan; and the Department of Molecular Oncology (M.S.), Graduate School of Medicine and Dentistry, Tokyo Medical and Dental University, Tokyo, Japan.

Correspondence to Kensuke Egashira, MD, PhD, Department of Cardiovascular Medicine, Graduate School of Medical Sciences, Kyushu University, 3-1-1, Maidashi, Higashi-ku, Fukuoka 812-8582, Japan. E-mail egashira@cardiol.med.kyushu-u.ac.jp

Arterioscler Thromb Vasc Biol **is available at http://atvb.ahajournals.org** **DOI: 10.1161/ATVBAHA.109.183772**

previous studies including ours, because sFlt-1 as well as other VEGF traps sequesters VEGF from its receptors nonspecifically.[2,10] It is reported that flk-1/KDR mainly mediates endothelial cell proliferation during angiogenesis,[11] so that flk-1 may promote reendothelialization and suppress neointima formation after injury. By contrast, flt-1 is reported to regulate nitric oxide production in endothelial cells,[12] and to regulate monocyte chemotaxis that may promote inflammation and influence neointima formation.[13] Therefore, the present study aimed to determine the relative role of each VEGF receptor, flt-1 versus flk-1, in neointima formation after vascular injury, using flt-1 tyrosine kinase-deficient (Flt-1 $TK^{-/-}$) mice[14] in the presence or absence of sFlt-1 gene transfer[2,15] in wire injury model.

Methods

Experimental Animals

All study protocols were reviewed and approved by the Committee on the Ethics of Animal Experiments in Kyushu University Graduate School of Medical Sciences. To examine the role of flt-1, we used Flt-1 $TK^{-/-}$ mice on C57Bl/6J background because flt-1 deficiency is known to be embryonic lethal.[14] Age-matched C57Bl/6J mice (CLEA Japan, Tokyo, Japan) were used as wild-type (WT) control. All mice were fed with normal diet and water at libitum.

Expression Vector

The 3.3-kb mouse *sFLT-1* gene, originally cloned from mouse lung cDNA library, was subcloned into the *Bam*H I (5′) and *Not* I (3′) sites of the eukaryotic expression vector cDNA3 plasmid (Invitrogen, Carlsbad, Calif).[2,16]

Femoral Arterial Wire Injury

To examine the role of flt-1 in neointima formation, femoral arterial wire injury was performed in male 12- to 20-week-old WT or Flt-1 $TK^{-/-}$ mice. After exposure of left femoral artery, straight spring wire (0.38 mm in diameter, COOK) was inserted into femoral artery from the muscular branch. The wire was placed for 1 minute to denude and dilate the artery. After removal of wire, branch artery was ligated and restoration of blood flow was verified by pulsation of peripheral arteries.[2,17] Twenty-eight days after injury, femoral artery was excised after injection of 10% buffered formalin and evaluated histopathologically. Heart rate and systolic blood pressure were measured by tail cuff method before sacrifice.

Soluble Flt-1 Gene Transfer

To examine the role of flk-1, sFlt-1 gene transfer was performed in Flt-1 $TK^{-/-}$ mice as described elsewhere.[2,4,15] Briefly, plasmid vector encoding sFlt-1 cDNA (100 μg) was injected in the gastrocnemial muscle followed by electroporation to facilitate gene transfer. sFlt-1 gene transfer was performed once every 2 weeks from 14 days before until 28 days after injury, based on the data that serum sFlt-1 concentration was elevated over 28 days after single injection of sFlt-1 plasmid with the peak at 14 day after injection (serum sFlt-1concentration at baseline and 3, 14, and 28 days after injection was 222±24, 396±59,* 970±55,* and 477±54* pg/mL, *$P<0.05$ versus baseline).

Histopathology and Immunohistochemistry

For histopathologic and immunohistochemical analysis, serial paraffin sections of the femoral artery were prepared. Briefly, femoral artery was excised after perfusion of 10% buffered formalin and fixed overnight in formalin. After fixation, the tissue was embedded in paraffin and cross sections (6 μm thick) were stained with Masson trichrome or elastica van Gieson stains. Neointima area was defined as the area surrounded by internal elastic lamina except lumen area. Extent of neointima formation was evaluated by the areal ratio of intima to media (I/M ratio) and neointima area. Other sections were subjected to immunostaining using rat anti-mouse macrophage monoclonal antibodies (Mac-3; BD Pharmingen), goat antimouse monocyte chemoattractant protein-1 (MCP-1) antibodies (Santa Cruz Biotechnology Inc). Proliferating cells were evaluated by the immunostaining with antiproliferating cell nuclear antigen (PCNA) antibody (DAKO). Alpha-smooth muscle actin (α-SMA, DAKO) and CD31 antibody (Santa Cruz) were also used as smooth muscle and endothelium marker. The respective nonimmune IgGs were used as negative controls. After incubation with biotinylated goat antirat IgG (Santa Cruz Biotechnology Inc) or rabbit anti-goat IgG (Nichirei), the sections were incubated with diaminobenzidine (DAB). The sections were then counterstained with Mayer hematoxylin. Analysis was performed using a microscope with a computerized, digital image analysis system and Scion Image Software (Scion Corporation). Fluorescent immunostaining was performed with secondary antibodies which are labeled by AlexaFluor 488 or 555 (Invitrogen).

Ex Vivo Culture of Mouse Aorta

Male 12- to 20-week-old WT Flt-1 $TK^{-/-}$ and sFlt-1 plasmid-injected Flt-1 $TK^{-/-}$ mice were used in this experiment. In the first experiment, sFlt-1 plasmid was injected 7 days before excision of aorta. Aorta was excised from ascending aorta to the bifurcation of iliac arteries and incubated with Dulbecco modified Eagle medium (DMEM) containing 1% fetal bovine serum (FBS). After overnight starvation, aorta was incubated with 50 ng/mL VEGF for 3 hours. Then, mRNA was extracted and quantitative real-time RT-PCR was performed by ABI PRISM 7000 Sequence Detection System (Applied Biosystems). MCP-1 and GAPDH primer, which is mixed with probes as TaqMan Gene Expression Assays, were commercially available and purchased from Applied Biosystems. The second experiment was performed using WT mice and blocking antibody of flt-1(R&D Systems Inc) and flk-1 (R&D Systems Inc). After overnight incubation with these antibodies, mRNA was collected in a similar fashion.

VEGF-Induced MCP-1 Expression in VSMCs

Mouse aortic VSMCs (P53LMACO1)[18] was purchased from Health Science Research Resource Banks and cultured in DMEM containing 10% FBS and phorbol-12myristate-13acetate (PMA, 100 nmol/L). VSMCs were used after 9 passages in the experiment. VSMCs were starved overnight and incubated with blocking antibody for flt-1 (10 μg/mL, R&D Systems) or flk-1 (1 μg/mL, R&D Systems). MCP-1 gene expression was analyzed by real-time PCR after 4-hour stimulation with 200 ng/mL human VEGF.

Peritoneal Macrophage Chemotaxis

Peritoneal fluid containing macrophage was harvested 4 days after intraperitoneal injection of thioglycolate. Macrophage migration was measured in 96-well chemotaxis chambers (Neuro Probe Inc). MCP-1 or VEGF in RPMI 1640 was added to the lower wells and the isolated macrophages (1×10^7 cells per mL) were placed in the upper wells. The concentration of MCP-1 and VEGF was 5, 15, and 50 ng/mL. After incubation for 90 minutes at 37°C, the upper surface of the membrane was washed with PBS and migrated cells on the lower surface were counted after staining with trypan blue. The number of cells per field was counted. All assays were performed in triplicate.

Statistics

All data are reported as the mean±SE. Statistical analysis of differences was performed by Student *t* test and 1-way ANOVA with Bonferroni post test. Statistical analysis of chemotaxis assay was performed by 2-way ANOVA with Bonferroni post test. Probability values less than 0.05 were considered to be statistically significant.

Results

Distinct Role of flt-1 and flk-1 in Neointima Formation After Wire Injury

To examine the role of flt-1 in neointima formation, we examined the degree of neointima formation after wire injury

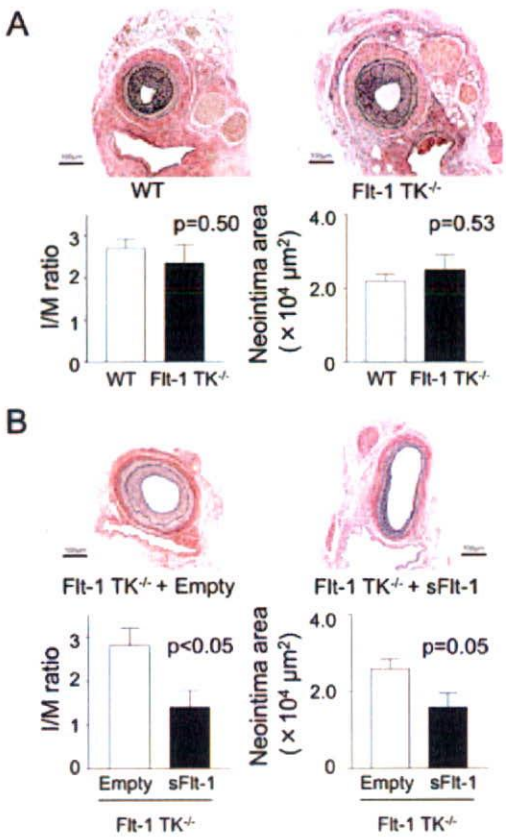

Figure 1. Distinct effects of flt-1 TK deficiency and sFlt-1 gene transfer on neointima formation. Neointima formation was comparable in wild-type (WT, n=7) and Flt-1 $TK^{-/-}$ mice (n=8) 28 days after wire injury (A). Neointima formation was significantly inhibited in Flt-1 $TK^{-/-}$ mice transfected with sFlt-1 plasmid (n=6) compared with empty plasmid (Empty, n=6; B). Scale bar indicates 100 μm.

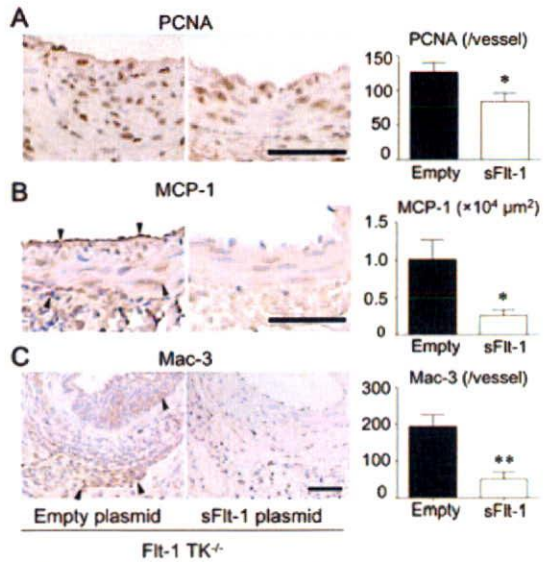

Figure 2. Gene transfer of sFlt-1 in Flt-1 $TK^{-/-}$ mice decreased PCNA-positive cells in the neointima (A), MCP-1 expression in the endothelial layer and medial cells (B), and Mac-3–positive monocytes/macrophages in the neointima and the adventitia (C) 7 days after injury (n=5 to 6 for each group). Scale bar indicate 50 μm. *$P<0.05$, **$P<0.01$ vs empty plasmid group. Arrowheads (▼) indicates stained cells.

in femoral arteries of Flt-1 $TK^{-/-}$ mice. Flt-1 $TK^{-/-}$ mice lack intracellular tyrosine kinase domain of flt-1 and thus downstream signaling.[14] Histological analysis revealed that there was no significant difference in I/M ratio and neointimal area 28 days after wire injury between WT and Flt-1 $TK^{-/-}$ mice (Figure 1A), suggesting that the role of flt-1 is minor in neointima formation in this model. Deficiency of flt-1 tyrosine kinase unaffected heart rate (673±11 versus 662±19 bpm) or blood pressure (110±3 versus 104±3 mm Hg) in mice, also unaffected macrophage infiltration evaluated as mac-3 staining, perivascular fibrosis and vessel diameter (data not shown).

To examine the role of flk-1, sFlt-1 gene transfer was performed into Flt-1 $TK^{-/-}$ mice. The sFlt-1 sequesters VEGF from both VEGF receptors and thus we could evaluate the role of flk-1 when applied to Flt-1 $TK^{-/-}$ mice. The sFlt-1 gene transfer markedly inhibited neointima formation with significant reduction of I/M ratio compared with control empty plasmid in Flt-1 $TK^{-/-}$ mice (Figure 1B). The sFlt-1 gene transfer did not affect heart rate (662±19 versus 660±11 bpm) and blood pressure (95±5 versus 107±4 mm Hg) in Flt-1 $TK^{-/-}$ mice.

sFlt-1 Gene Transfer Suppressed Proliferation, Monocyte Infiltration, and MCP-1 Expression in Flt-1 $TK^{-/-}$ Mice

We have repeatedly shown the importance of MCP-1 and monocyte-mediated inflammation in the vascular wall during vascular remodeling in various vascular disease models.[19–22] Thus, we analyzed the effect of sFlt-1 gene transfer on proliferation of vascular wall cells, MCP-1 expression, and monocyte/macrophage infiltration at an early stage of neointima formation. Histology at 7 days after injury showed a decrease in PCNA-positive cells in the neointima of Flt-1 $TK^{-/-}$ mice transfected with sFlt-1 gene that underpins reduction in neointima formation (Figure 2A). Prominent MCP-1 induction was found in the intimal and the medial cells in Flt-1 $TK^{-/-}$ mice, which was markedly suppressed by sFlt-1 gene transfer (Figure 2B). Infiltration of Mac-3–positive monocytes was found in the media and adventitia, which was suppressed by sFlt-1 gene transfer as well (Figure 2C). These results suggest that endogenous VEGF upregulates MCP-1 and macrophage recruitment via flk-1 in Flt-1 $TK^{-/-}$ mice during neointima formation after wire injury.

Distinct Role of flt-1 and flk-1 in VEGF-Mediated MCP-1 Induction

To elucidate detailed mechanisms of VEGF-mediated MCP-1 induction in injured arteries, we first performed double immunostaining of MCP-1 and α-SMA 3 days after injury when the endothelium has not regenerated yet. We found equivalent MCP-1 induction in the medial VSMCs in WT and Flt-1 $TK^{-/-}$ mice. In contrast, sFlt-1 gene transfer into Flt-1 $TK^{-/-}$ mice remarkably inhibited MCP-1 induction (Figure 3A). These results suggest that (1) wire injury induces MCP-1 expression primarily in the VSMCs and (2) flk-1, but not

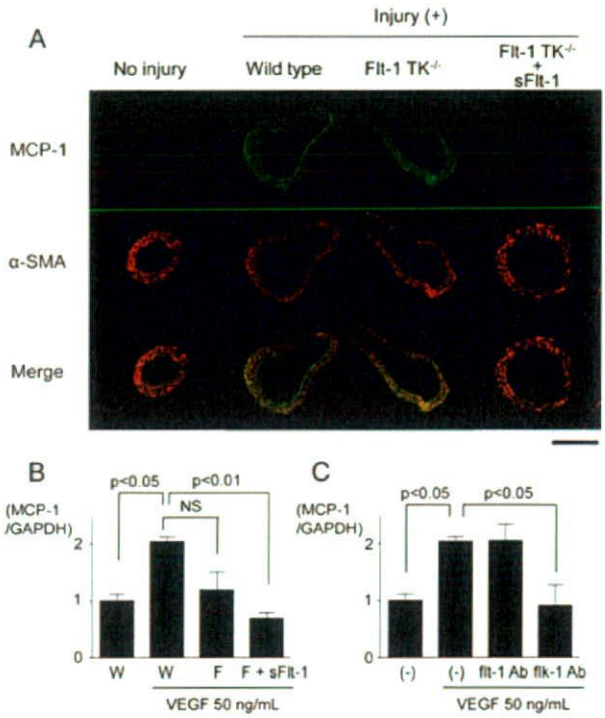

Figure 3. Blockade of flk-1 suppressed MCP-1 induction in VSMCs in vivo and ex vivo. Immunostaining of MCP-1 and α-SMA revealed that MCP-1 is induced in the medial VSMCs 3 days after injury (A). Scale indicates 200 μm. VEGF-induced MCP-1 expression in cultured aortas was inhibited by sFlt-1 gene transfer (B, n=3 each) and anti–flk-1 antibody (C, n=3 each). W: wild type mice, F: Flt-1 $TK^{-/-}$ mice.

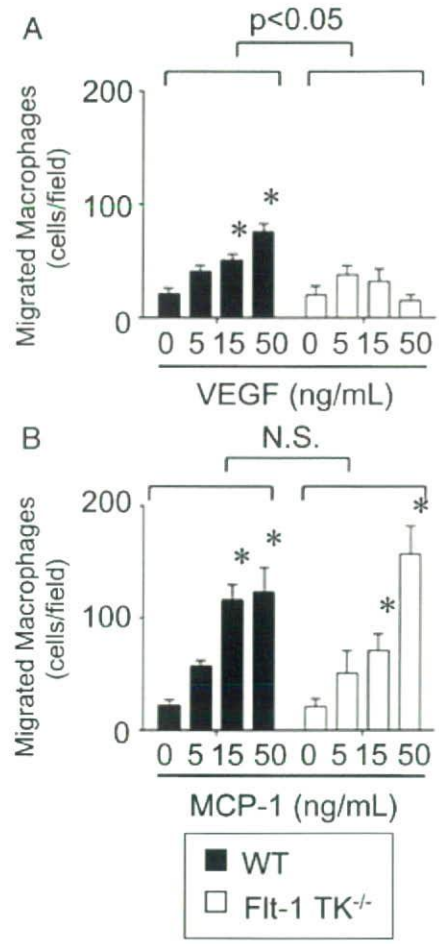

Figure 4. Flt-1 TK deficiency blunted VEGF-induced chemotaxis of macrophages. Chemotaxis of peritoneal macrophage to VEGF or MCP-1 was examined in Boyden chamber experiments. VEGF induced significant chemotaxis in WT mice, which was blunted in Flt-1 $TK^{-/-}$ mice (A). MCP-1 induced prominent and equivalent chemotaxis in WT and Flt-1 $TK^{-/-}$ mice (B). n=6 to 7 for each group. *$P<0.05$ vs control.

flt-1, mediates MCP-1 induction in the VSMCs immediately after vascular injury. Next, we examined the role of each VEGF receptor in MCP-1 induction in ex vivo culture model. Mouse aorta was harvested from WT, Flt-1 $TK^{-/-}$, and sFlt-1 plasmid-administrated Flt-1 $TK^{-/-}$ mice. The aortas were stimulated with VEGF (50 ng/mL) after 24-hour starvation, and induction of MCP-1 was quantified by real-time PCR. Real-time PCR showed that VEGF-induced expression of MCP-1, which is partially but not significantly inhibited by Flt-1 TK deletion and is completely inhibited by sFlt-1 gene transfer, suggesting that VEGF-induced MCP-1 mRNA transcription is primarily mediated by flk-1 (Figure 3B). Blockade of each VEGF receptor by neutralizing antibodies showed that anti–flt-1 antibody had no effect; by contrast, anti–flk-1 antibody completely inhibited VEGF-induced MCP-1 expression (Figure 3C). Finally we examined the effect of each VEGF receptor blockade on VEGF-induced MCP-1 expression in mouse aortic VSMCs. Blocking antibody of flt-1 did not inhibit VEGF-induced MCP-1 expression. In contrast, blocking antibody of flk-1 significantly inhibited VEGF-induced MCP-1 expression (supplemental Figure I, please see http://atvb.ahajournals.org). These results suggest that VEGF induces MCP-1 expression by flk-1–mediated mechanisms in mouse VSMCs. We also examined whether blockade of VEGF influences PDGF signaling that may mediate MCP-1 induction in injured arterial wall.[23] In vitro study using cultured VSMCs revealed that blockade of VEGF by sFlt-1 gene transfer or sFlt-1 protein does not inhibit PDGF-induced phosphorylation of PDGF receptors, suggesting that blockade of flk-1 inhibit MCP-1 induction via PDGF-independent mechanisms (supplemental Figure II).

Macrophage Chemotaxis in WT and Flt-1 $TK^{-/-}$ Mice

It is reported that human monocytes exclusively express flt-1 and that VEGF induces chemotaxis by flt-1–mediated mechanism.[13] We performed Boyden chamber experiment to examine macrophage chemotactic function in response to VEGF or MCP-1 in WT and Flt-1 $TK^{-/-}$ mice. VEGF induced significant chemotaxis of peritoneal macrophage from WT mice, which was abolished by Flt-1 TK deficiency (Figure 4A), suggesting that flt-1 essentially mediates VEGF-induced chemotaxis. By contrast, MCP-1 caused more prominent chemotaxis in WT and Flt-1 $TK^{-/-}$ mice equivalently (Figure 4B). These results suggest that MCP-1–induced chemotaxis was preserved in Flt-1 $TK^{-/-}$ mice, and MCP-1 is a primary mediator of flk-1–dependent macrophage recruitment in injured vascular wall even in the Flt-1 TK deficiency.

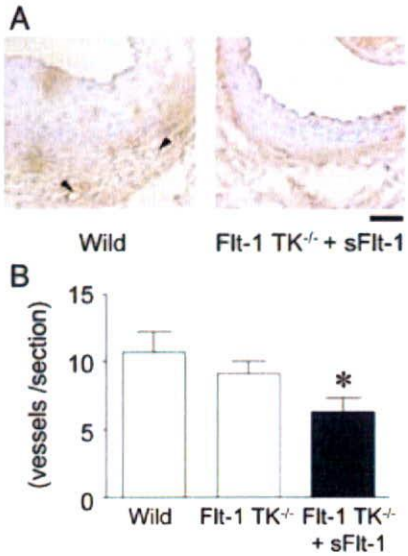

Figure 5. Adventitial angiogenesis was evaluated by CD31 immunostaining 28 days after wire injury (A). sFlt-1 gene transfer into Flt-1 $TK^{-/-}$ mice inhibited adventitial angiogenesis compared with wild mice (B). n=7 for each group. *$P<0.05$ versus wild type.

Effect of sFlt-1 Gene Transfer on Adventitial Angiogenesis

Adventitial angiogenesis was evaluated by counting CD31-positive endothelial cells in the adventitia of injured femoral arteries. Adventitial angiogenesis was equivalent in WT and Flt-1 $TK^{-/-}$ mice, however, was significantly decreased in Flt-1 $TK^{-/-}$ mice after sFlt-1 gene transfer compared with WT mice (Figure 5).

Discussion

In this study, we aimed to clarify the relative importance of 2 VEGF receptors, flt-1 and flk-1/KDR in neointima formation after intraluminal wire injury. Major findings were: (1) Flt-1 TK deficiency unaffected neointima formation, (2) sFlt-1 gene transfer into Flt-1 $TK^{-/-}$ mice remarkably suppressed neointima formation, and (3) VEGF induced MCP-1 expression in VSMCs which was blocked by flk-1–specific antibody. The inhibition of neointima formation by flk-1 blockade was preceded by significant reduction of MCP-1 expression in the medial VSMCs 3 days after injury, and monocyte infiltration, VSMC proliferation, and perivascular neovascularization 7 days after injury. These in vivo results suggest that flk-1 plays a primary role in the development of neointima by regulating macrophage-mediated inflammation in this model.

Inflammation in the vascular wall, mainly mediated by monocyte and macrophage, is a hallmark of vascular remodeling after injury as evident in our previous studies using cuff injury in mice and balloon injury in rats, rabbits, and monkeys, in which MCP-1 blockade effectively suppresses vascular inflammation and remodeling.[24–26] It is reported that VEGF induces MCP-1 expression in endothelial cells[27]; in turn, MCP-1 induces VEGF in VSMCs.[28] Macrophage-mediated inflammation activates VSMC migration and proliferation by cytokines, or by redox-dependent signaling.[29,30]

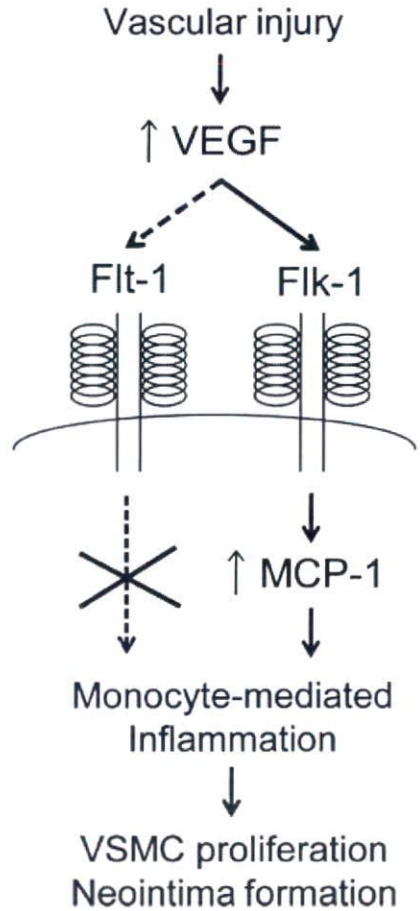

Figure 6. Flk-1 accelerates neointima formation after vascular injury. VEGF is upregulated in vascular wall cells after wire injury. VEGF activates flk-1 to cause MCP-1 induction and monocyte recruitment to the injured vascular wall. Monocyte/macrophage-mediated inflammation results in VSMC proliferation and neointima formation. Flt-1–mediated monocyte chemotaxis is minor to cause neointima formation in vivo, as indicated by dotted lines.

Although flk-1 is expressed mainly in endothelial cells, VSMCs also express flk-1,[31] and the present study revealed a new mechanism that flk-1 mediates MCP-1 expression in VSMCs and monocyte recruitment after injury. This VEGF/MCP-1–positive feedback and downstream signaling is considered to be a major underlying mechanism in neointima formation after injury, as shown in our previous studies using sFlt-1 and MCP-1 mutant[19,24–26] (Figure 6).

It has been reported that VEGF induces direct macrophage chemotaxis by flt-1–mediated mechanisms, whereas flk-1 is not expressed on monocytes/macrophages.[13] Indeed, Flt-1 TK deficiency abrogated VEGF-induced chemotaxis in peritoneal macrophages in the present study; however, Flt-1 TK deficiency had no effect on macrophage infiltration into injured arterial wall and neointima formation in in vivo setting. In the present study, blockade of flk-1 inhibited MCP-1 expression in the medial VSMCs and abrogated monocyte accumulation in the vascular wall after injury. Thus, we considered that MCP-1, which is regulated by VEGF/flk-1 pathway, mainly mediates macrophage chemo-

taxis rather than VEGF/flt-1 expressed on monocyte itself. This mechanism well explains the in vivo effect of flk-1 blockade on monocyte accumulation after injury.

In the present study, sFlt-1 gene transfer also inhibited adventitial angiogenesis after injury. Inhibition of adventitial angiogenesis may be another mechanism by which flk-1 blockade inhibits neointima formation, because a positive correlation was observed between adventitial blood vessel formation and neointima formation in various injury model including rabbit collar placement model.[32]

The role of VEGF in neointima formation may be different depending on the mode of injury or the species studied. For example, Isner et al[33] reported that local delivery of VEGF accelerates reendothelialization and attenuates intimal hyperplasia in balloon-injured rat carotid artery. Hutter et al[5] reported in mouse wire injury model that intravenous injection of VEGF adenovirus promoted endothelial repair and inhibited neointima formation. By contrast, Khurana et al[32] reported that adenovirus-mediated VEGF gene transfer exacerbates adventitial neovascularization and neointima formation in rabbit periadventitial collar replacement model, which was abrogated by administration of sFlt-1. Thus, there remain controversies in the role of VEGF gene transfer per se in neointima formation in previous studies. In the present study, we administered sFlt-1 plasmid intramuscularly, and sFlt-1, which was detected in the serum, blocked VEGF signaling at the site of vascular injury. In our previous study, we have reported that reendothelialization is complete 14 days after wire injury in mice irrespective of VEGF blockade by sFlt-1 gene transfer.[2] Thus, it is suggested that on complete reendothelialization, excess VEGF may accelerate neointima formation by promoting monocyte-mediated inflammation through flk-1–dependent MCP-1 expression in the injured vascular wall at least in the murine wire injury model studied. In this situation, Flk-1–specific VEGF blockade may be another potential approach to control vascular inflammation and subsequent remodeling after injury.

In conclusion, the present study demonstrated that soluble sFlt-1 gene transfer ameliorates neointima formation after wire injury in flt-1 tyrosine kinase–deficient mice by inhibiting MCP-1 expression in the medial VSMCs and resulting monocyte-mediated inflammation. The present findings suggest that endogenous VEGF accelerates neointima formation after injury through flk-1–dependent mechanisms, and provide new insights into complex VEGF-mediated signaling in vascular remodeling.

Sources of Funding

This study was supported by Grants-in-Aid for Scientific Research (19390216, 19650134) from the Ministry of Education, Science, and Culture, Tokyo, Japan and by Health Science Research Grants (Research on Translational Research and Nano-medicine) from the Ministry of Health Labor and Welfare, Tokyo, Japan.

Disclosures

None.

References

1. Brasen JH, Kivela A, Roser K, Rissanen TT, Niemi M, Luft FC, Donath K, Yla-Herttuala S. Angiogenesis, vascular endothelial growth factor and platelet-derived growth factor-BB expression, iron deposition, and oxidation-specific epitopes in stented human coronary arteries. *Arterioscler Thromb Vasc Biol.* 2001;21:1720–1726.
2. Ohtani K, Egashira K, Hiasa K, Zhao Q, Kitamoto S, Ishibashi M, Usui M, Inoue S, Yonemitsu Y, Sueishi K, Sata M, Shibuya M, Sunagawa K. Blockade of vascular endothelial growth factor suppresses experimental restenosis after intraluminal injury by inhibiting recruitment of monocyte lineage cells. *Circulation.* 2004;110:2444–2452.
3. Shibata M, Suzuki H, Nakatani M, Koba S, Geshi E, Katagiri T, Takeyama Y. The involvement of vascular endothelial growth factor and flt-1 in the process of neointimal proliferation in pig coronary arteries following stent implantation. *Histochem Cell Biol.* 2001;116:471–481.
4. Zhao Q, Egashira K, Hiasa K, Ishibashi M, Inoue S, Ohtani K, Tan C, Shibuya M, Takeshita A, Sunagawa K. Essential role of vascular endothelial growth factor and Flt-1 signals in neointimal formation after periadventitial injury. *Arterioscler Thromb Vasc Biol.* 2004;24:2284–2289.
5. Hutter R, Carrick FE, Valdiviezo C, Wolinsky C, Rudge JS, Wiegand SJ, Fuster V, Badimon JJ, Sauter BV. Vascular endothelial growth factor regulates reendothelialization and neointima formation in a mouse model of arterial injury. *Circulation.* 2004;110:2430–2435.
6. Bhardwaj S, Roy H, Heikura T, Yla-Herttuala S. VEGF-A, VEGF-D and VEGF-D(DeltaNDeltaC) induced intimal hyperplasia in carotid arteries. *Eur J Clin Invest.* 2005:669–676.
7. Hedman M, Hartikainen J, Syvanne M, Stjernvall J, Hedman A, Kivela A, Vanninen E, Mussalo H, Kauppila E, Simula S, Narvanen O, Rantala A, Peuhkurinen K, Nieminen MS, Laakso M, Yla-Herttuala S. Safety and feasibility of catheter-based local intracoronary vascular endothelial growth factor gene transfer in the prevention of postangioplasty and in-stent restenosis and in the treatment of chronic myocardial ischemia: phase II results of the Kuopio Angiogenesis Trial (KAT). *Circulation.* 2003;107:2677–2683.
8. Laitinen M, Hartikainen J, Hiltunen MO, Eranen J, Kiviniemi M, Narvanen O, Makinen K, Manninen H, Syvanne M, Martin JF, Laakso M, Yla-Herttuala S. Catheter-mediated vascular endothelial growth factor gene transfer to human coronary arteries after angioplasty. *Hum Gene Ther.* 2000;11:263–270.
9. Shiojima I, Walsh K. The role of vascular endothelial growth factor in restenosis: the controversy continues. *Circulation.* 2004;110:2283–2286.
10. Kendall RL, Wang G, Thomas KA. Identification of a natural soluble form of the vascular endothelial growth factor receptor, FLT-1, and its heterodimerization with KDR. *Biochem Biophys Res Commun.* 1996;226:324–328.
11. Millauer B, Wizigmann-Voos S, Schnurch H, Martinez R, Moller NP, Risau W, Ullrich A. High affinity VEGF binding and developmental expression suggest Flk-1 as a major regulator of vasculogenesis and angiogenesis. *Cell.* 1993;72:835–846.
12. Bussolati B, Dunk C, Grohman M, Kontos CD, Mason J, Ahmed A. Vascular endothelial growth factor receptor-1 modulates vascular endothelial growth factor-mediated angiogenesis via nitric oxide. *Am J Pathol.* 2001;159:993–1008.
13. Barleon B, Sozzani S, Zhou D, Weich HA, Mantovani A, Marme D. Migration of human monocytes in response to vascular endothelial growth factor (VEGF) is mediated via the VEGF receptor flt-1. *Blood.* 1996;87:3336–3343.
14. Hiratsuka S, Minowa O, Kuno J, Noda T, Shibuya M. Flt-1 lacking the tyrosine kinase domain is sufficient for normal development and angiogenesis in mice. *Proc Natl Acad Sci U S A.* 1998;95:9349–9354.
15. Zhao Q, Ishibashi M, Hiasa K, Tan C, Takeshita A, Egashira K. Essential role of vascular endothelial growth factor in angiotensin II-induced vascular inflammation and remodeling. *Hypertension.* 2004;44:264–270.
16. Kondo K, Hiratsuka S, Subbalakshmi E, Matsushime H, Shibuya M. Genomic organization of the flt-1 gene encoding for vascular endothelial growth factor (VEGF) receptor-1 suggests an intimate evolutionary relationship between the 7-Ig and the 5-Ig tyrosine kinase receptors. *Gene.* 1998;208:297–305.
17. Sata M, Maejima Y, Adachi F, Fukino K, Saiura A, Sugiura S, Aoyagi T, Imai Y, Kurihara H, Kimura K, Omata M, Makuuchi M, Hirata Y, Nagai R. A mouse model of vascular injury that induces rapid onset of medial cell apoptosis followed by reproducible neointimal hyperplasia. *J Mol Cell Cardiol.* 2000;32:2097–2104.
18. Masuda T, Ohmi K, Yamaguchi H, Hasegawa K, Sugiyama T, Matsuda Y, Iino M, Nonomura Y. Growing and differentiating characterization of aortic smooth muscle cell line, p53LMAC01 obtained from p53 knock out mice. *Mol Cell Biochem.* 1999;190:99–104.

19. Egashira K. Molecular mechanisms mediating inflammation in vascular disease: special reference to monocyte chemoattractant protein-1. *Hypertension*. 2003;41:834–841.
20. Egashira K, Nakano K, Ohtani K, Funakoshi K, Zhao G, Ihara Y, Koga J, Kimura S, Tominaga R, Sunagawa K. Local delivery of anti-monocyte chemoattractant protein-1 by gene-eluting stents attenuates in-stent stenosis in rabbits and monkeys. *Arterioscler Thromb Vasc Biol*. 2007;27:2563–2568.
21. Inoue S, Egashira K, Ni W, Kitamoto S, Usui M, Otani K, Ishibashi M, Hiasa K, Nishida K, Takeshita A. Anti-monocyte chemoattractant protein-1 gene therapy limits progression and destabilization of established atherosclerosis in apolipoprotein E-knockout mice. *Circulation*. 2002;106:2700–2706.
22. Nakano K, Egashira K, Ohtani K, Zhao G, Funakoshi K, Ihara Y, Sunagawa K. Catheter-based adenovirus-mediated anti-monocyte chemoattractant gene therapy attenuates in-stent neointima formation in cynomolgus monkeys. *Atherosclerosis*. 2007;194:309–316.
23. Marumo T, Schini-Kerth VB, Fisslthaler B, Busse R. Platelet-derived growth factor-stimulated superoxide anion production modulates activation of transcription factor NF-kappaB and expression of monocyte chemoattractant protein 1 in human aortic smooth muscle cells. *Circulation*. 1997;96:2361–2367.
24. Egashira K, Zhao Q, Kataoka C, Ohtani K, Usui M, Charo IF, Nishida K, Inoue S, Katoh M, Ichiki T, Takeshita A. Importance of monocyte chemoattractant protein-1 pathway in neointimal hyperplasia after periarterial injury in mice and monkeys. *Circ Res*. 2002;90:1167–1172.
25. Ohtani K, Usui M, Nakano K, Kohjimoto Y, Kitajima S, Hirouchi Y, Li XH, Kitamoto S, Takeshita A, Egashira K. Antimonocyte chemoattractant protein-1 gene therapy reduces experimental in-stent restenosis in hypercholesterolemic rabbits and monkeys. *Gene Ther*. 2004;11:1273–1282.
26. Usui M, Egashira K, Ohtani K, Kataoka C, Ishibashi M, Hiasa K, Katoh M, Zhao Q, Kitamoto S, Takeshita A. Anti-monocyte chemoattractant protein-1 gene therapy inhibits restenotic changes (neointimal hyperplasia) after balloon injury in rats and monkeys. *Faseb J*. 2002;16:1838–1840.
27. Yamada M, Kim S, Egashira K, Takeya M, Ikeda T, Mimura O, Iwao H. Molecular mechanism and role of endothelial monocyte chemoattractant protein-1 induction by vascular endothelial growth factor. *Arterioscler Thromb Vasc Biol*. 2003;23:1996–2001.
28. Parenti A, Bellik L, Brogelli L, Filippi S, Ledda F. Endogenous VEGF-A is responsible for mitogenic effects of MCP-1 on vascular smooth muscle cells. *Am J Physiol Heart Circ Physiol*. 2004;286:H1978–H1984.
29. Griendling KK, FitzGerald GA. Oxidative stress and cardiovascular injury: Part I: basic mechanisms and in vivo monitoring of ROS. *Circulation*. 2003;108:1912–1916.
30. Viedt C, Vogel J, Athanasiou T, Shen W, Orth SR, Kubler W, Kreuzer J. Monocyte chemoattractant protein-1 induces proliferation and interleukin-6 production in human smooth muscle cells by differential activation of nuclear factor-kappaB and activator protein-1. *Arterioscler Thromb Vasc Biol*. 2002;22:914–920.
31. Ishida A, Murray J, Saito Y, Kanthou C, Benzakour O, Shibuya M, Wijelath ES. Expression of vascular endothelial growth factor receptors in smooth muscle cells. *J Cell Physiol*. 2001;188:359–368.
32. Khurana R, Zhuang Z, Bhardwaj S, Murakami M, De Muinck E, Yla-Herttuala S, Ferrara N, Martin JF, Zachary I, Simons M. Angiogenesis-dependent and independent phases of intimal hyperplasia. *Circulation*. 2004;110:2436–2443.
33. Asahara T, Bauters C, Pastore C, Kearney M, Rossow S, Bunting S, Ferrara N, Symes JF, Isner JM. Local delivery of vascular endothelial growth factor accelerates reendothelialization and attenuates intimal hyperplasia in balloon-injured rat carotid artery. *Circulation*. 1995;91:2793–2801.

Circ J 2009; **73:** 381–383

Intracardiac Echocardiography-Guided Cardiac Tumor Biopsy

Taiki Higo, MD; Masao Takemoto, MD; Kiyohiro Ogawa, MD; Shujiro Inoue, MD; Ken-ichi Eshima, MD; Hideo Tada, MD; Kenji Sunagawa, MD

A 63-year-old woman was admitted to hospital with the chief complaint of new onset chest discomfort and pretibial pitting edema. Transthoracic echocardiography revealed a large invasive tumor on the heart protruding into the right atrium and right ventricle, which obstructed the outflow tract. She underwent transvenous 9Fr, 9-MHz ultra intracardiac echocardiography (ICE) (EP Technologies, Boston Scientific Corporation, San Jose, CA, USA) guided biopsy, and a diagnosis of malignant lymphoma was established from the specimen obtained. ICE-guided cardiac tumor biopsy may be one of the most useful strategies for diagnosis of cardiac tumors. (*Circ J* 2009; **73:** 381–383)

Key Words: Biopsy; Cardiac tumor; Diagnosis; Intracardiac echocardiography; Malignant lymphoma

Although primary cardiac tumors are relatively rare[1] physicians unexpectedly encounter them in clinical practice and it is important to establish a histopathological diagnosis in order to treat them adequately; however, it is difficult to do so non-invasively. We describe a case of a primary cardiac malignant lymphoma that was easily and safely diagnosed histopathologically after a transvenous intracardiac echocardiography (ICE)-guided biopsy.

Case Report

A 63-year-old woman was admitted to hospital with the chief complaint of new onset chest discomfort and pretibial pitting edema. On physical examination, dilated jugular veins and pretibial pitting edema were noted. Auscultation revealed a cardiac ejection systolic murmur and normal vesicular lung sounds. Chest X-ray revealed cardiomegaly (cardiothoracic ratio=64%), and the electrocardiogram demonstrated right-axis deviation, right bundle blanch block, low voltage in the limb leads, and poor R wave progression in the precordial leads. Transthoracic echocardiography (TTE) revealed a large invasive cardiac tumor protruding into the right atrium (RA) and right ventricle (RV), obstructing the outflow tract (RVOT) (**Figs 1A,B**). There was also moderate pericardial effusion without any hemodynamic significance. Contrast computed tomography (CT) also showed the large cardiac tumor measuring 76×37 mm in diameter and stretching from the RA to the RV and pulmonary artery (**Fig 2**). Pericardial effusion, as

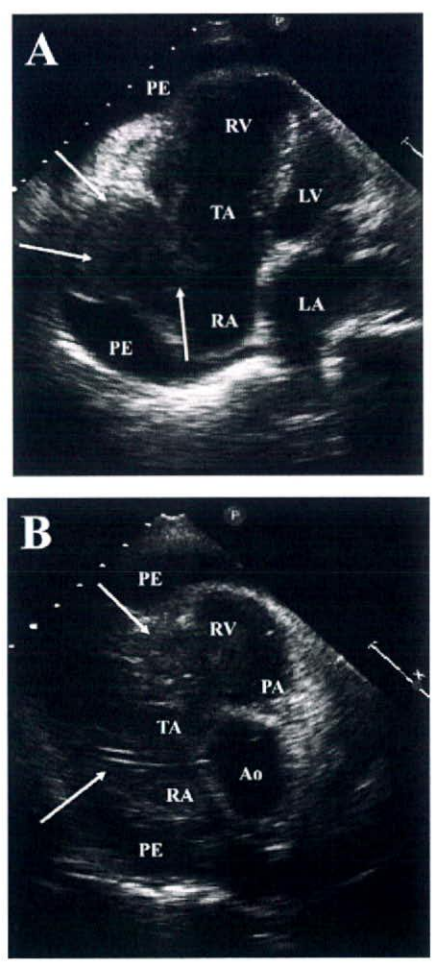

Fig 1. Two-dimensional transthoracic echocardiograms on admission in the apical 4-chamber view (**A**) and short-axis view (**B**) show the large invasive cardiac tumor (white arrows) protruding into the right atrium (RA) and right ventricle (RV), and causing an RV outflow tract obstruction. PA, pulmonary artery; PE, pericardial effusion; TA, tricuspid valve annulus; LA, left atrium; LV, left ventricle; Ao, aorta.

(Received January 15, 2008; revised manuscript received March 5, 2008; accepted April 29, 2008; released online December 5, 2008)
Department of Cardiovascular Medicine, Kyushu University Hospital, Fukuoka, Japan
There is no conflict of interest related to this study.
Mailing address: Masao Takemoto, MD, Department of Cardiovascular Medicine, Kyushu University Hospital, 3-1-1 Maidashi, Higashi-ku, Fukuoka 812-8582, Japan. E-mail: matakemo@cardiol.med.kyushu-u.ac.jp

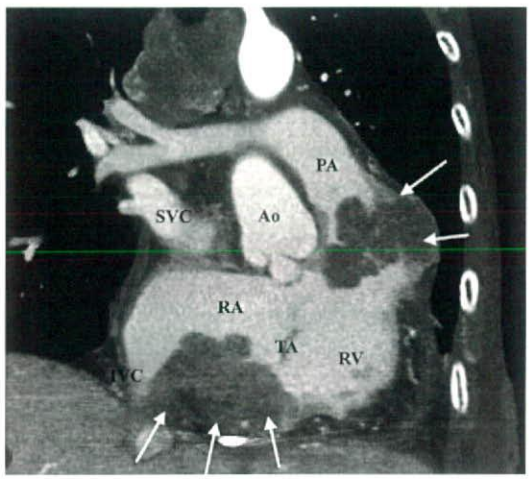

Fig 2. Contrast computed tomographic image shows the cardiac tumor (white arrows) protruding into the right atrium (RA) and right ventricle (RV), and causing an RV outflow tract obstruction. Ao, aorta; PA, pulmonary artery; TA, tricuspid valve annulus; SVC, superior vena cava; IVC, inferior vena cava.

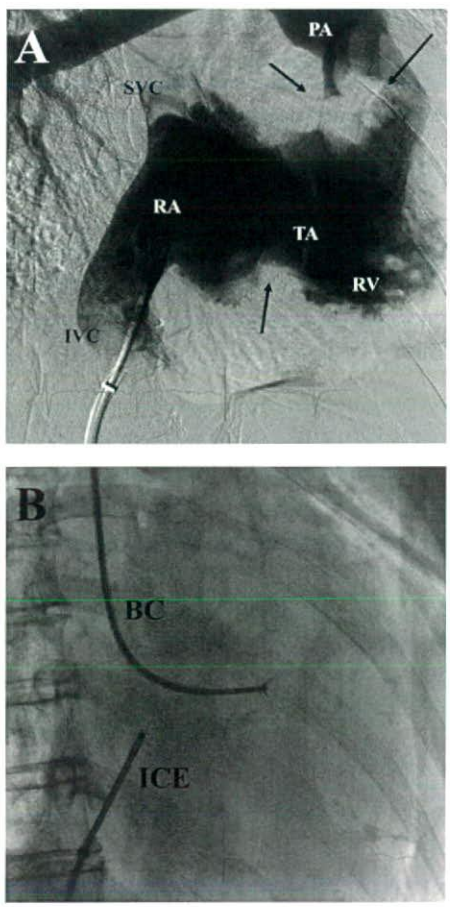

Fig 3. Right anterior oblique (RAO) view of a right atriogram (**A**) showing the cardiac tumor (black arrows) protruding into the right atrium (RA) and right ventricle (RV), and causing an RV outflow tract obstruction. RAO view of a fluoroscopic image (**B**) shows the location of the biopsy catheter (BC) next to the cardiac tumor and the intracardiac echocardiography (ICE) catheter in the RA. PA, pulmonary artery; TA, tricuspid valve annulus; SVC, superior vena cava; IVC, inferior vena cava.

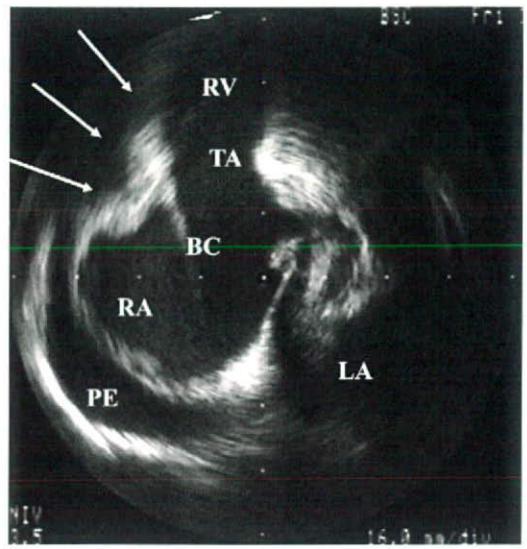

Fig 4. Intracardiac echocardiographic image shows the biopsy catheter (BC) next to the cardiac tumor (white arrows) protruding into the right atrium (RA) and right ventricle (RV). PE, pericardial effusion; TA, tricuspid valve annulus; LA, left atrium.

well as mediastinal and mesenteric lymphadenopathy, were revealed. Because the cytology examination from the pericardial effusion was negative, a percutaneous cardiac tumor biopsy was performed in order to establish a histopathological diagnosis. Right atriography also revealed the cardiac tumor protruding into the RA and RV (**Fig 3A**). A 6Fr cardiac biopsy catheter (Technowood Biopsy Forceps, Tonokura Ika Kogyo Co Ltd, Tokyo, Japan) and 9Fr, 9-MHz Ultra ICE catheter (EP Technologies, Boston Scientific Corporation, San Jose, CA, USA) were percutaneously inserted into the RA via the right jugular vein and right femoral vein, respectively (**Fig 3B**). Because ICE images enabled detailed examination of the intracardiac structures, as well as an accurate surveillance of the positioning of the biopsy catheter (**Fig 4**), cardiac tumor specimens were easily and safely taken without any complications, pain, or exposure of the echocardiographer to radiation. Histopathological analysis showed diffuse large B-cell lymphoma. The patient underwent R-THPCOP chemotherapy (rituximab, pirarubicin, cyclosporin, vincristine, and prednisolone). During the first month following the treatment, her condition improved, which correlated with the finding of a decrease in the tumor size, and resolution of the pericardial effusion and RVOT obstruction on TTE. She has remained well under chemotherapy as an outpatient.

Discussion

Primary cardiac tumors are relatively rare with an incidence of 0.002–0.3% in autopsy series;[1] however, physicians unexpectedly encounter them in clinical practice and although the exact incidence of each specific tumor type can not be stated, approximately 75% of all cardiac tumors are histologically benign and the remainder are malignant.[2] Sarcomas are the most common malignant primary cardiac tumors and primary cardiac lymphomas are much less common,[3] with a relative incidence of only 2% of primary cardiac tumors.

The available and useful noninvasive diagnostic tools

such as echocardiography, CT, and magnetic resonance imaging can provide much important information regarding the size, shape, composition, attachment, and surface characteristics of tumors[4,5] which are important considerations for surgical excision, but surgery is not an effective treatment for the great majority of malignant cardiac tumors, because of the large mass of cardiac tissue involved, as in the present case, and because all cardiac tumors have the potential for causing life-threatening complications[6] including embolization. Thus, it is critically important to establish a histopathlogical diagnosis for instigation of appropriate treatment as soon as possible.

Previous reports demonstrate that a transvenous biopsy under TTE or transesophageal echocardiographic (TEE) guidance[4,7,8] is a useful diagnostic approach. Although TTE is the most noninvasive and convenient technique, TEE can provide superior imaging to TTE, especially of posteriorly located structures[9] However, TEE sometimes causes the patient pain if performed without anesthesia, and for that reason it may usually requires local pharyngeal anesthesia and sometimes general sedation. Moreover, the operator of the TTE or TEE is at risk of exposure to radiation during the procedure.

ICE is a new technique based on the use of an ultrasonic diagnostic catheter that can be introduced through the femoral vein and provides a 2-dimensional view[10] Image acquisition is usually from within the RA or RV. Thus, ICE enables complete examination of the inter-atrial and -ventricular structures, as well as an accurate surveillance of the positioning of intracardiac devices[11] such as a biopsy catheter. A major advantage of ICE is its potential to provide superior information to TEE,[10,11] as well as avoiding general sedation and exposure of the echocardiographer to radiation. Therefore, ICE may be one of the most useful diagnostic strategies and should be considered when trying to diagnose the histopathology of cardiac tumors. At present, however, the main limiting factor is its high cost, which is related to the single-use catheters.

Acknowledgments

We thank Kazutaka Yamaguchi for his technical assistance for intracardiac echocardiography, and John Martin for his linguistic assistance with this paper.

References

1. Reynen K. Frequency of primary tumors of the heart. *Am J Cardiol* 1996; **77:** 107.
2. Lam KY, Dickens P, Chan AC. Tumors of the heart: A 20-year experience with a review of 12,485 consecutive autopsies. *Arch Pathol Lab Med* 1993; **117:** 1027–1031.
3. Kasai K, Kuwao S, Sato Y, Murayama M, Harano Y, Kameya T. Case report of primary cardiac lymphoma: The applications of PCR to the diagnosis of primary cardiac lymphoma. *Acta Pathol Jpn* 1992; **42:** 667–671.
4. Abramowitz Y, Hiller N, Perlman G, Admon D, Beeri R, Chajek-Shaul T, et al. The diagnosis of primary cardiac lymphoma by right heart catheterization and biopsy using fluoroscopic and transthoracic echocardiographic guidance. *Int J Cardiol* 2007; **118:** e39–e40.
5. Sato Y, Matsumoto N, Kinukawa N, Matsuo S, Komatsu S, Kunimasa T, et al. Successful treatment of primary cardiac B-cell lymphoma: Depiction at multislice computed tomography and magnetic resonance imaging. *Int J Cardiol* 2006; **113:** E26–E29.
6. Harvey WP. Clinical aspects of cardiac tumors. *Am J Cardiol* 1968; **21:** 28–43.
7. Kang SM, Rim SJ, Chang HJ, Choi D, Cho SY, Cho SH, et al. Primary cardiac lymphoma diagnosed by transvenous biopsy under transesophageal echocardiographic guidance and treated with systemic chemotherapy. *Echocardiography* 2003; **20:** 101–103.
8. Jurkovich D, de Marchena E, Bilsker M, Fierro-Renoy C, Temple D, Garcia H. Primary cardiac lymphoma diagnosed by percutaneous intracardiac biopsy with combined fluoroscopic and transesophageal echocardiographic imaging. *Catheter Cardiovasc Interv* 2000; **50:** 226–233.
9. Edwards LC 3rd, Louie EK. Transthoracic and transesophageal echocardiography for the evaluation of cardiac tumors, thrombi, and valvular vegetations. *Am J Card Imaging* 1994; **8:** 45–58.
10. Girod G, Delabays A, Roguelov C, Renders F, Van de Walle S, Vogt P, et al. Intracardiac echocardiography: A new tool for interventional cardiology. *Rev Med Suisse* 2007; **3:** 1696–1701.
11. Brochet E, Habib G. Intracardiac echocardiography during percutaneous closure of atrial septal defect and patent foramen ovale. *Arch Mal Coeur Vaiss* 2005; **98:** 25–28.

Free Radical Research, January 2009; 43(1): 37–46

informa
healthcare

Time-dependent changes of myocardial and systemic oxidative stress are dissociated after myocardial infarction

TAKAHIRO INOUE[1], TOMOMI IDE[1], MAYUMI YAMATO[2], MASAYOSHI YOSHIDA[1], TAKAKI TSUTSUMI[1], MAKOTO ANDOU[1], HIDEO UTSUMI[3], HIROYUKI TSUTSUI[4], & KENJI SUNAGAWA[1]

[1]*Department of Cardiovascular Medicine, Graduate School of Medical Sciences,* [2]*Department of REDOX Medicinal Science,* [3]*Department of Bio-functional Science, Graduate School of Pharmaceutical Sciences, Kyushu University, Fukuoka 812-8582, Japan, and* [4]*Department of Cardiovascular Medicine, Hokkaido University Graduate School of Medicine, Sapporo 060-8638, Japan*

Accepted by Professor G. Mann

(Received 10 July 2008; revised 17 September 2008)

Abstract

Reactive oxygen species (ROS) is increased in myocardium after myocardial infarction (MI), which may play a causal role in cardiac remodelling. However, there is scant direct and longitudinal evidence that systemic oxidative stress is enhanced accompanying an increase of ROS in myocardium. The authors conducted a comprehensive investigation of ROS markers by simultaneously sampling urine, blood and myocardium and *in vivo* ESR for the heart at different stages of post-MI cardiac remodelling in mouse with permanent occlusion of left coronary artery. Systemic oxidative markers increased at early days after MI and were normalized later. In contrast, TBARS and 4-hexanoyl-Lys staining were increased in non-infarct myocardium at day 28. The enhancement of ESR signal decay of methoxycarbonyl-PROXYL measured at the chest was associated with the progression of left ventricle dilatation and dysfunction. This study provided the direct evidence that redox alteration and production of ROS occurred in myocardium during the progression of cardiac remodelling and failure; however, ROS marker levels in blood and urine do not reflect the production of ROS from failing myocardium.

Keywords: *Myocardial remodelling, oxidative stress markers, heart failure, in vivo ESR*

Abbreviations: *LV, left ventricular; MI, myocardial infarction; HF, heart failure; RAS, renin-angiotensin system; ROS, reactive oxygen species; MMP, matrix metalloproteinase; TBARS, thiobarbituric acid reactive substances; 8-OH-dG, 8-hydroxy-2′-deoxyguanosine; GPx, glutathione peroxidase; SOD, superoxide dismutase; HEL, Nε-(Hexanoyl) Lysin; ESR, electron spin resonance; FS, fractional shortening; HR, heart rate; LVEDD, left ventricular end-diastolic dimension; LVESD, left ventricular end-systolic dimension; 3-methoxycarbonyl-PROXYL, 3-methoxycarbonyl-2,2,5,5-tetramethylpyrrolidine-1-oxyl*

Introduction

Pathological left ventricular (LV) remodelling after myocardial infarction (MI) is increasingly recognized as the major cause of heart failure (HF) [1]. MI induces alterations of LV architecture with scar formation, ventricular dilatation and hypertrophy of the non-infarct myocardium [2]. In the process of remodelling, activation of various neurohumoral factors and inflammatory response, including activation of the

Correspondence: Tomomi Ide, MD, PhD, Department of Cardiovascular Medicine, Kyushu University Graduate School of Medicine, 3-1-1, Maidashi, Higashi-ku, Fukuoka 812-8582, Japan. Tel: +81-92-642-5360. Fax: +81-92-642-5374. Email: tomomi_i@cardiol.med.kyushu-u.ac.jp

ISSN 1071-5762 print/ISSN 1029-2470 online
DOI: 10.1080/10715760802534820

renin-angiotensin system (RAS), contributes to healing and scar formation in the infarct myocardium. At the end of the repairing process, cardiac hypertrophy due to haemodynamic overload is associated with hypertrophic growth of cardiomyocytes accompanying fibrosis and inappropriate interstitial collagen formation. The prognosis of HF remains poor even with wide use of RAS inhibitors and β adrenergic receptor blockers [3]. Recently, growing evidence has suggested that reactive oxygen species (ROS) are involved in the pathophysiology of myocardial remodelling and failure [4–10] and increases of ROS have been shown in various animal models of HF. We and others have demonstrated that generation of ROS is increased in post-MI myocardium in mice [9] and that treatment with antioxidants or over-expression of antioxidant enzymes prevents cardiac remodelling [11–13], resulting in improvement of survival after MI [12,13]. *In vitro* experiments demonstrated that ROS mediate hypertrophy in cardiomyocytes induced by neurohumoral factors such as angiotensin II and catecholamines, as well as cytokines including TNFα [14–17]. ROS modulate extracellular matrix function via their effects on fibroblast proliferation and collagen synthesis, involving redox-sensitive activation of matrix metalloproteinases (MMPs) [11,18,19]. Moreover, ROS alter gene expression in the case of intracellular Ca^{2+} overload, activating various proteases and promoting apoptosis in cardiomyocytes [20,21]. The above findings thus strongly suggest that redox regulation may be a potential therapeutic strategy for cardiac remodelling and HF. However, despite much discussion on the biological activities of ROS in remodelling, there is scanty clinical or animal experimental evidence for elevation of systemic oxidative biomarkers corresponding to the increase of ROS in the remodelling myocardium. We thus examined the time courses of oxidative stress in the post-MI myocardium and in systemic circulation by performing simultaneous sampling of urine, blood and myocardium during the post-MI course in a HF mouse model. Since the effects of ROS depend on a balance between the pro-oxidant molecules generated and the antioxidant reserve *in vivo*, both components should be tested to obtain better understanding of the effects of ROS on the progression of remodelling. For a comprehensive investigation of oxidative stress, we measured the byproducts of ROS represented by thiobarbituric acid reactive substances (TBARS) and 8-hydroxy-2′-deoxyguanosine (8-OH-dG), as well as the antioxidant defense capacity indicated by scavenger enzymes. Moreover, excised biological specimens only enable one to identify the target of ROS after the exposure to ROS but not to reflect the dynamic changes of redox status *in vivo* in the chronic HF model. Accordingly, we applied *in vivo* ESR to estimate redox status non-invasively in the process of remodelling using a post-MI HF model in mice.

Materials and methods

Animal model

This experiment conformed with the Guide for the Care and Use of Laboratory Animals published by the US National Institute of Health and was reviewed and approved by the Committee of the Ethics on Animal Experiment, Kyushu University Graduate School of Medical Sciences, and performed in compliance with the relevant Law (No. 105) and Notification (No. 6) of the Japanese Government.

Six week-old CD-1 male mice were purchased from Kyudo Co., Ltd. (Saga, Japan). The mice were housed in a temperature- and humidity-controlled room. MI was experimentally induced in mice by ligating the left coronary artery permanently, as previously reported [11]. The mice were assigned randomly into five groups; post-MI days 1, 4, 7, 14 and 28, and the survived mice (survived/operated: $n = 6/7$, 6/8, 10/14, 9/11, 14/21, respectively) were used in the experiments on the assigned days. Urine, blood and myocardium samples were collected from each mouse. The myocardial samples of all six mice on post-MI day 4 and six mice on post-MI day 28 were examined immunohistochemically, while the samples of the other mice were used for biochemical analysis. The data were compared with those from control mice that underwent sham operation without coronary artery ligation at day 28 ($n = 7$).

Echocardiography and haemodynamic measurements

Echocardiographic studies were performed under light anaesthesia by an intraperitoneal injection of sodium pentobarbital, with spontaneous respiration before the animal was euthanized. A 2D parasternal short-axis view of the LV was obtained by applying the transducer lightly to the mid-upper left anterior chest wall. The transducer was then gently moved cephalad or caudad and angulated until desirable images were obtained. After ensuring that the image was on axis (based on roundness of the LV cavity), 2D targeted M-mode tracings were recorded at a paper speed of 50 mm/s. Our previous study showed small intra-observer and inter-observer variabilities of our echocardiographic measurements for LV dimensions and high reproducibility of measurements made in the same animals on separate days [22]. Under the same anaesthesia with Avertin, a 1.4 Fr micromanometer-tipped catheter (Millar Instruments) was inserted into the right carotid artery and then advanced into the LV for the measurement of LV pressures for the assessment of severity of HF at day 28 after MI.

Blood sampling

Blood sample was collected with 1:500 dilution of heparin just before euthanizing each animal. Plasma was separated by centrifugation at $1000 \times g$ for 15 min at 4°C and stored at −80°C until analysis. The erythrocyte fraction was washed three times with isotonic NaCl. A stock haemolysate was prepared by the addition of the 2-mercaptoethanol-EDTA stabilizing solution. The concentrated haemolysate was diluted with 2% ethanol immediately before assay.

TBARS in plasma and 8-OH-dG in urine

To assess the level of systemic oxidative stress generated in the process of cardiac remodelling after MI, we measured TBARS in plasma and 8-OH-dG in urine. Plasma TBARS was measured by fluorometric analysis. The plasma was pre-treated with 10% phosphotungstic acid and 1/12 N sulphuric acid. The sample was mixed with a reagent to obtain a final concentration of 7.5% acetic acid, 2 mmol/L EDTA and 0.4% SDS and then reacted with 0.3% thiobarbituric acid (TBA) in a boiling water bath for 45 min. After cooling, the chromogen was extracted in n-butanol/pyridine (15:1, v/v). Fluorescence of the supernatant was measured at excitation and emission wavelengths of 510 and 550 nm, respectively, using a GENios Pro™ (Tecan Group Ltd. Durham, NC). The standard was prepared using 1,1,3,3, -tetraethoxypropane (TEP).

Urine samples were collected in individual metabolic cages (Nalgen, Rochester, NY). After overnight fasting, urine sample was collected from each mouse. Urine 8-OH-dG concentration was determined using a competitive ELISA kit (8-OH-dG check®, Japan, Institute for the Control of Aging, Nagoya, Japan). The value was corrected by urinary creatinine measured with a colorimetric assay kit (Sigma, St. Louis, MO).

TBARS in myocardial tissue

The myocardium was homogenized in 10 volumes of 50 mmol/L sodium phosphate buffer at 4°C for the assay of TBARS in myocardium. The homogenate was centrifuged at $4500 \times g$ for 15 min and the supernatant was used for the biochemical assay of TBARS as in plasma.

Antioxidant enzyme activities in myocardium

To determine the change in capacity of defense during the progression of cardiac remodelling, we measured the levels of antioxidant enzyme activities in the myocardium.

The enzymatic activities of glutathione peroxidase (GPx) and superoxide dismutase (SOD) were measured spectrophotometrically (Tecan Group Ltd., GENios). GPx activity was determined according to the method of Yamamoto and Takahashi [23] by following the oxidation of NADPH in the presence of GR (Oriental Yeast Co., Ltd. Tokyo, Japan), which catalyses the reduction of oxidized glutathione (GSSH) formed by GPx. One enzyme unit is defined as the amount of enzyme that oxidizes 1 μmol of NADPH per minute. SOD activity was examined by the cytochrome c method, in which xanthine and xanthine oxidase (Oriental Yeast Co., Ltd. Tokyo, Japan) were used as a source of superoxide. A unit was defined as the quantity of SOD required for 50% inhibition of the rate of cytochrome c reduction (Wako Pure Chemical Industries, Inc. Osaka, Japan). Protein concentration was determined by the Bradford assay.

Hexanoyl-Lysine adduct (HEL) immunostaining in myocardial tissue

Left ventricular myocardial sections obtained from mice at baseline, day 3 and 28 after MI were immunolabelled by a specific monoclonal anti-HEL antibody (Nikkenn SEIL Corp.). Paraffin-embedded tissue sections (5-μm thick) were deparaffinized with xylene, refixed in Bouin's solution for 20 min, immersed in PBS, incubated with 0.3% H_2O_2 in methanol for 30 min, followed by blocking with M.O.M. mouse IgG blocking reagent. The sections were further incubated with monoclonal anti-HEL antibody in M.O.M. Diluent. After rinsing with 10 mmol/L PBS, they were incubated with biotin-labelled goat anti-rabbit IgG anti-serum (1:100 dilution; DAKO A/S) for 60 min and then with avidin-biotin complex (1:100 dilution; Vectastain ABC kit) for 60 min. After rinsing, the sections were finally incubated with 0.02% 3,3-diaminobenzidine and 0.03% H_2O_2 in deionized water for 6–9 min. As a negative control, sections were incubated with normal rabbit serum instead of anti-HEL antibody.

In vivo *electron spin resonance study*

A spin probe, 3-methoxycarbonyl-2,2,5,5-tetramethylpyrrolidine-1-oxyl (methoxycarbonyl-PROXYL) was synthesized as described previously [24]. For the *in vivo* ESR measurements, 100 mmol/L isotonic methoxycarbonyl-PROXYL was administered (3 μl/g body weight) in mice intravenously. Then ESR spectra were taken at regular intervals using a L-band ESR spectrometer (JEOL Co. Ltd., Akishima, Japan) with a loop-gap resonator (33 mm i.d. and 30 mm in length), as reported previously [25,26]. The power of the 1.1 GHz microwave was 10 mW. The amplitude of the 100-kHz field modulation was 0.063 mT. The signal decay rates, which were used as an index of ROS generation, were determined from the semi-logarithmic plots of signal